이학석사 학위논문

오염된 매질에서 V형 신경 작용제 모방체를 신속하고 선택적으로 검출하기 위한 고분자 필름

Thin Colorimetric Film Array for Rapid and Selective Detection of V-type Nerve Agent Mimic in Potentially Contaminated Areas

울산대학교 대학원

화 학 과

박 소 영

Thin Colorimetric Film Array for Rapid and Selective Detection of V-type Nerve Agent Mimic in Potentially Contaminated Areas

지도교수 이 형 일

이 논문을 이학석사학위 논문으로 제출함

2024년 02월

울 산 대 학 교 대 학 원

화 학 과

박 소 영

박소영의 석사학위 논문을 인준함

심사위원 이형일 인

심사위원 이승구 인

심사위원 김범진 인

울 산 대 학 교 대 학 원

2024년 02월

Contents ····· 1

Abstract

The expeditious detection and quantification of V-series nerve agents (VX) on potentially contaminated surfaces are crucial for the prevention of regional conflict incidents, acts of terrorism, or illicit activities. However, the low volatility and high toxicity of VX make these tasks challenging. Herein, we designed two novel colorimetric thin polymeric films to rapidly and sensitively detect demeton-S, a VX mimic, in contaminated areas. The polymeric films were specifically engineered to include a coordination site for Au (III) ions. Initially, these films were coordinated with Au (III), causing a discernible alteration in color due to enhancement in intramolecular charge transfer process. In the presence of demeton-S, the Au (III) ligands in the films are displaced with demeton-S, resulting in the restoration of the original color of the film, as the enhanced intramolecular charge transfer process is inhibited and thereby serving as an indicator of the presence of demeton-S. The polymeric films exhibit remarkable selectivity toward demeton-S compared to G-type nerve agents and other interference. The reusability of the polymeric films for demeton-S detection was achieved owing to the reversibility of the films during the alternative exposure of Au (III) and demeton-S. The polymeric films demonstrated their applicability for demeton-S detection and quantification in several contaminated areas, including different water, soil, and skin, rendering them highly suitable for on-site measurements.

Keywords: *colorimetric, polymeric film, nerve agent, VX mimic, displacement*

1. Introduction

Chemical warfare agents represent a menacing category of weapons that are capable of inflicting catastrophic harm on military personnel and civilian populations.[1-3] Among them, nerve agents have garnered considerable attention owing to their unparalleled potency and the lethal consequences they inflict upon exposure.[4] Nerve agents comprise a class of organophosphate compounds that induce disturbances in the regular operation of the nervous system, causing a series of profound physiological and neurological consequences.[5, 6] Historically, nerve agents have been categorized into two major types: G and V series. G series, including sarin (GB), tabun, soman, and cyclosarin, were initially developed and employed during the 20th century.[7, 8] Extensive research has been performed on these G agents, providing a better understanding of their properties, action mechanisms, and potential countermeasures.[9]

However, recent concerns have emerged regarding the increasing prevalence and risks associated with V-type nerve agents.[10] The V-series nerve agents, specifically VX, RVX, and CVX, are characterized by their heightened persistence and toxicity in comparison to G compounds.[11] For instance, when comparing GB and VX, it is estimated that the toxicity of VX is approximately twice when inhaled, ten times when orally administered, and 170 times when administered through dermal exposure.[12] Furthermore, it is currently predicted that the LD_{50} values for humans through percutaneous exposure are 3-10 mg/man for VX and 1700 mg/man for GB.[13, 14] Due to its immediate lethality and toxicity upon contact or inhalation, active research has been performed on detection using demeton-S, a V-series nerve agent surrogate with similar activity but relatively lower toxicity.[15, 16]

Traditionally, various techniques including ion mobility spectroscopy, electrochemical sensors, enzyme-based biosensors, high-performance liquid chromatography, and gas chromatography have been employed in research endeavors to identify and quantify nerve agents.[17-19] Most of these methods possess the drawback of requiring operators with extensive training and monitoring systems. The aforementioned limitations have prompted a surge of interest in the utilization of fluorescent and chromogenic chemical sensors as a viable substitute for instrumental methodologies.[20, 21] Optical sensors exhibit several distinct advantages in comparison to instrumental methods, including uncomplicated visual detection in the field and eliminating the necessity for sample preparation or intricate equipment.[22, 23] Furthermore, chemical sensors offer portability, rapid response times, real-time monitoring capabilities, cost-effectiveness, and the ability to qualitatively or quantitatively detect substances.[24, 25] Additionally, chemical sensors exhibit ease of reaction, along with high selectivity and sensitivity.[26, 27] Nevertheless, although there is considerable literature on chemical sensors designed to detect G-type nerve agents, the availability of chemical sensor probes specifically tailored for V-type

nerve agents remains extremely limited.[28, 29]

Furthermore, efficient heterogeneous sensors are in demand for practical applications in the field, requiring the immediate detection of even small amounts of residues.[30] Polymeric films have garnered considerable interest within the realm of sensor technology owing to their notable attributes, including heightened selectivity, enhanced structural stability, and cost-effectiveness.[31, 32] Although several sensing systems have been developed for individual analyte detection, there is a need for the development of polymeric films capable of simultaneous or continuous multianalyte detection.[33] Multianalyte detection can be achieved by introducing a single reaction/binding site that continuously detects multiple analytes.[34] Various mechanisms have been proposed to achieve continuous detection, including coordination of metal ions and their replacement with an analyte.[35] In this case, the continuous detection of two analytes must be reversible, such that the entire process can be repeated over several cycles.[36, 37] Polymeric films are highly advantageous for this application owing to their ability to be repeatedly reused without compromising their stability.[38]

In this work, we present the development of two colorimetric thin polymeric films tailored to sensitively detect demeton-S within contaminated environments. To achieve this, the polymeric films were strategically engineered with a coordination site for Au (III) ions and integrated azobenzene-based signaling structures, modified with diverse pendant-R groups, including hydrogen and aldehydes, to render the sensitivity of the film. The experimental process involved coordinating the polymeric films with Au (III), leading to a noticeable color change. When exposed to demeton-S, the Au (III) displacement mechanism within the films caused a restoration of their original color, thereby serving as an indicator of the presence of demeton-S. The suitability of the polymeric films for on-site measurements in various affected media and surfaces, such as water, soil, and skin, was demonstrated, highlighting their potential for demeton-S detection (Scheme 1).

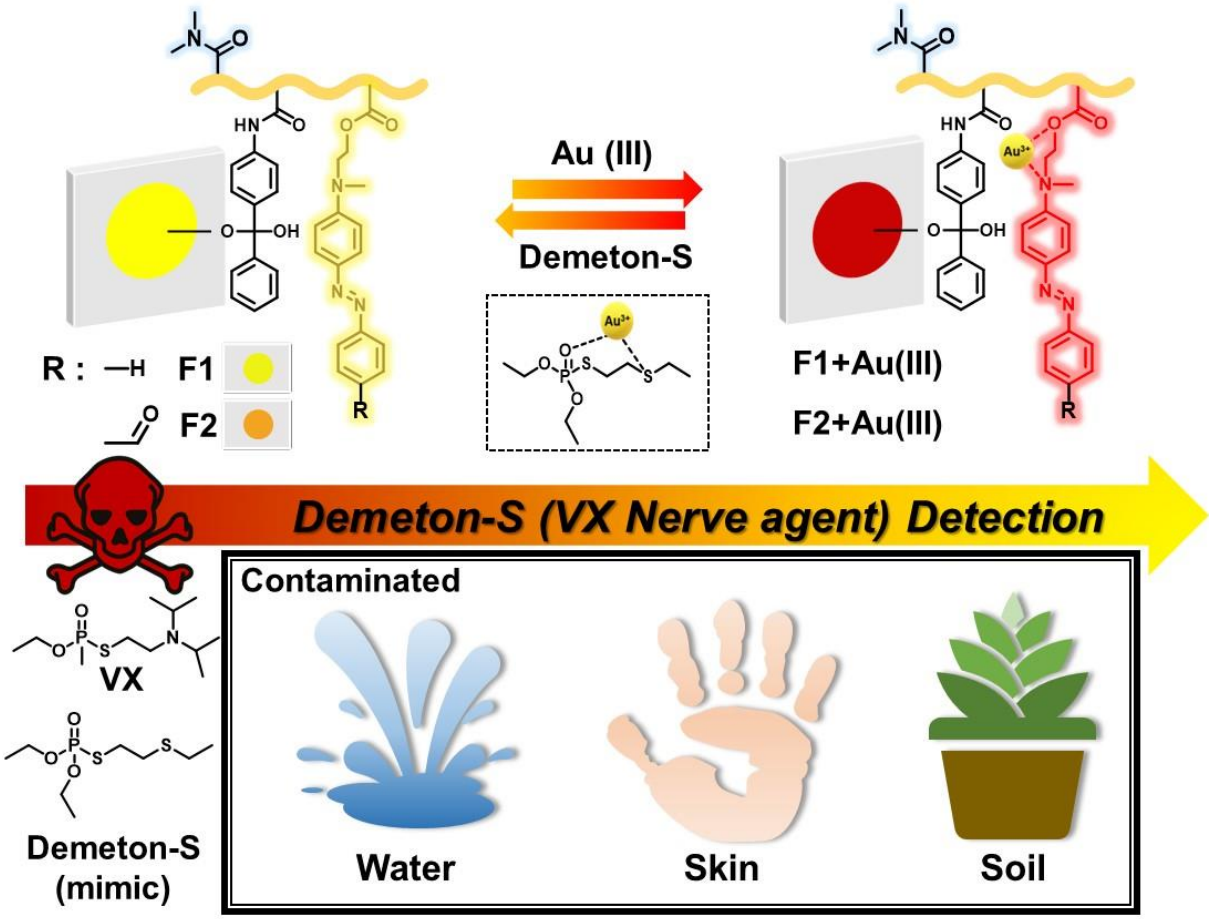

Scheme 1. Au (III) coordinated polymeric films for demeton-S detection in various contaminated areas at 25ºC and 60 % relative humidity.

2. Experimental

Chemicals and materials

Acrylic acid, aniline, sodium nitrite, urea (99%), butyl lithium (2.5 M in Hexane), diethyl chlorophosphite (DCP, 97%), diethyl cyanophosphonate (DCNP, 90%), triethyl phosphite (TEP, 98%), and gold (III) chloride trihydrate (99%) were purchased from Aldrich. The 2,2′-azobis-(isobutyronitrile) (AIBN, Aldrich, 98%) was recrystallized from ethanol. 4-Aminobenzaldehyde (98%), *N,N*′-dimethylacrylamide (DMA, 99%), *N*-(3-dimethylaminopropyl)-3-ethylcarbodiimide hydrochloride (EDC·HCl, 98%), 4-dimethylaminopyridine (DMAP, 99%), 2-(*N*-methylanilino)ethanol (97%), and iodoethane (99%) were purchased from TCI, Korea. The iodoethane and DMA was passed through a basic alumina column to remove stabilizers. Dimethyl methylphosphonate (DMMP, 97%), 1,2-ethanedithiol (98%), and tin (II) chloride dihydrate (98%) were purchased from Alfa Aesar. Sodium bicarbonate and sodium hydroxide (98%) were purchased from SAMCHUN, Korea. Tributyl phosphate (TBP) was purchased from DAEJUNG. *N*-(4-benzoylphenyl)acrylamide (BPAm) was synthesized as previously reported. The solvent utilized in the NMR study, $CDCl_3$ (99%, D), was procured from Cambridge Isotope Laboratories, Inc., USA.

Instrumentation

^{1}H NMR measurements in $CDCl_3$ were recorded on a Bruker Vance 400 MHz. The determination of apparent molecular weights and the polydispersity index (PDI) of polymers was performed through gel permeation chromatography (GPC, Agilent Technologies 1200 series). The experiment was performed with the aid of a poly(methyl methacrylate) (PMMA) standard in DMF at a temperature of 30°C and a flow rate of 1 mL/min. Absorption spectra in the UV–vis range were captured using a Varian Cary 100 UV–vis spectrophotometer. The immobilization of the polymer-coated film onto the quartz slide was achieved using a light source comprising a medium-pressure 125-W Hg lamp, which was equipped with a 365-nm wavelength filter.

Synthesis

2-(ethylthio)ethanethiol

A round-bottomed flask was charged with 1.27 g (31.8 mmol) of sodium hydroxide and 40 mL of anhydrous dichloromethane. At 0°C, the solution was supplemented with 1,2-ethanedithiol (10 g, 106 mmol). A solution of iodoethane (8.27 g, 53 mmol) in DCM was added in a dropwise manner. The reaction mixture underwent a 15-min argon purging process and was subjected to overnight reflux. The solvent was evaporated to obtain a residue, which was subsequently poured into water, and the resulting product was subjected to two rounds of extraction using DCM. The colorless liquid product was purified via silica gel column chromatography using hexane/ethyl acetate (3:1, v/v) as an eluent.

^{1}H NMR (CDCl3, ppm), δ: 2.85–2.65 (m, 4H, –CH_2–CH_2); 2.62–2.50 (m, 2H, –CH_2); 1.65 (s, 1H, -SH); 1.32–1.20 (t, 3H, –CH_3)

Demeton-S

A mixture containing 2-(ethylthio) ethanethiol (2 g, 16 mmol) dissolved in 20 mL of ethyl acetate was cooled in an ice–acetone bath for 5 min. The solution was treated with 6.4 mL of butyl lithium, which had a concentration of 2.5 M in hexane. The solution of diethyl chlorophosphite in ethyl ether (10 mL) was introduced into the suspension under ice–acetone bath conditions. The mixture underwent stirring at 25°C for 3 h. Subsequently, the precipitate was separated from the reaction mixture via filtration, and the resultant liquid mixture was subjected to evaporation. The colorless liquid product was obtained with a 76% yield after purification of the residue through silica gel column chromatography, using hexane–ethyl acetate (1:1, v/v) as an eluent.

^{1}H NMR ($CDCl_3$, ppm), δ: 4.30–4.12 (m, 4H, –CH_3); 3.12–2.90 (m, 2H, –CH_2–); 2.87–2.77 (m, 2H, –CH_2); 2.55–2.60 (q, 2H, –CH_2); 1.45–1.32 (t, 6H, –CH_3); 1.30–1.20 (t, 3H, –CH_3).

2-(Methyl(phenyl)amino)ethyl acrylate was synthesized as reported previously. ^{1}H NMR ($CDCl_3$, ppm), δ: 7.35–7.21 (m, 2H), 7.26 (d, 2H), 6.78 (d, 1H), 6.36 (d, 1H), 6.17 (d, 1H), 5.87 (d, 1H), 4.41 (t, 2H), 3.68 (t, 2H), 3.01 (s, 3H).

(E)-2-(Methyl(4-(phenyldiazenyl)phenyl)amino)ethyl acrylate (M1) was synthesized as reported previously.[35] ^{1}H NMR ($CDCl_3$, ppm), δ: 7.92–6.75 (m, 9H, Ar–H); 6.42–5.78 (m, 3H, vinyl H); 4.38

(t, 2H, O–CH_2–); 3.75 (t, 2H, N–CH_2); 3.11 (s, 3H, CH_3).

(E)-2-((4-(4-Formylphenyl)diazenyl)phenyl)(methyl)amino)ethyl acrylate (M2) was synthesized as reported previously. ^{1}H NMR ($CDCl_3$, ppm), δ: 10.0 (s, 1H, –CHO); 8.05–6.78 (m, 8H, Ar–H); 6.45–5.80 (m, 3H, vinyl H); 4.39 (t, 2H, O–CH_2–); 3.77 (t, 2H, N–CH_2); 3.13 (s, 3H, CH_3).

p(DMA-*co*-M1-*co*-BPAm), P1 / p(DMA-*co*-M2-*co*-BPAm), P2

Polymeric probes P1 and P2 were synthesized via the free radical polymerization (FRP). In a 10-mL Schlenk flask DMA (1.96 mL, 19 mmol), M1 (250 mg, 0.81 mmol) / M2 (273 mg, 0.81 mmol), BPAm (102 mg, 0.40 mmol), and AIBN (16.6 mg, 0.10 mmol) were added. A total of 10 mL of anhydrous DMF was introduced and subjected to a 20-min purging process with dry argon gas. The purpose of this procedure was to eliminate any traces of oxygen present in the system. The solution mixture was subjected to thermal treatment by placing it in a preheated environment at a temperature of 70°C for 14 h. The polymerization process was terminated by cooling; the flask was immersed in an ice bath and the solution was subsequently exposed to air. The precipitation of the reaction solution was performed thrice using diethyl ether. The solid obtained from the experiment was collected through filtration and subsequently subjected to drying in a vacuum oven at a temperature of 30°C.

P1 yellow solid: ^{1}H NMR ($CDCl_3$, ppm), δ: 7.92–6.65 (m, 14H, Ar–H); 4.22 (m, 2H, O–CH_2–); 3.65 (m, 2H, N–CH_2); 3.35–2.21 (m, 10H, N–CH_3, N–$(CH_3)_2$ and–C–O–NH), GPC: Mn = 30310 Da, Mw = 48830 Da and PDI = 1.61.

P2 orange solid: ^{1}H NMR ($CDCl_3$, ppm), δ: 10.0 (s, 1H, CHO), 8.0−6.5 (m, 17H, Ar−H), 4.17 (m, 2H, O−CH_2−), 3.65 (m, 2H, N−CH_2), and 3.26−1.02 (m, 12H, N−$(CH_3)_2$ and aliphatic H from DMA, Azo−CHO). Mn = 31000 Da, Mw = 52320 Da, and PDI = 1.68.

Estimation of limit of detection (LOD)

The limit of detection was determined by Eq. (1):

$LOD = 3\sigma/K$……(1)

where K is the slope of the curve, and σ is the standard deviation.

Estimation of Binding Constant

The binding association constant (Ka) or displacement constant (K_d) of the reaction between F1 or F2 and Au(III) followed by demeton-S was calculated from the UV–vis titration data according to the Benesi–Hildebrand equation, given here as Eq. (2) or (3):

$$\frac{1}{A\text{-}A_0} = \frac{1}{K(A_{max}\text{-}A_0)[Au^{3+}]} + \frac{1}{A_{max}\text{-}A_0}, \quad (2)$$

$$A_{max}/(A_{max}\text{-}A) = 1/A + 1/K_a.1/[Q] \quad (3)$$

3. Results and discussion

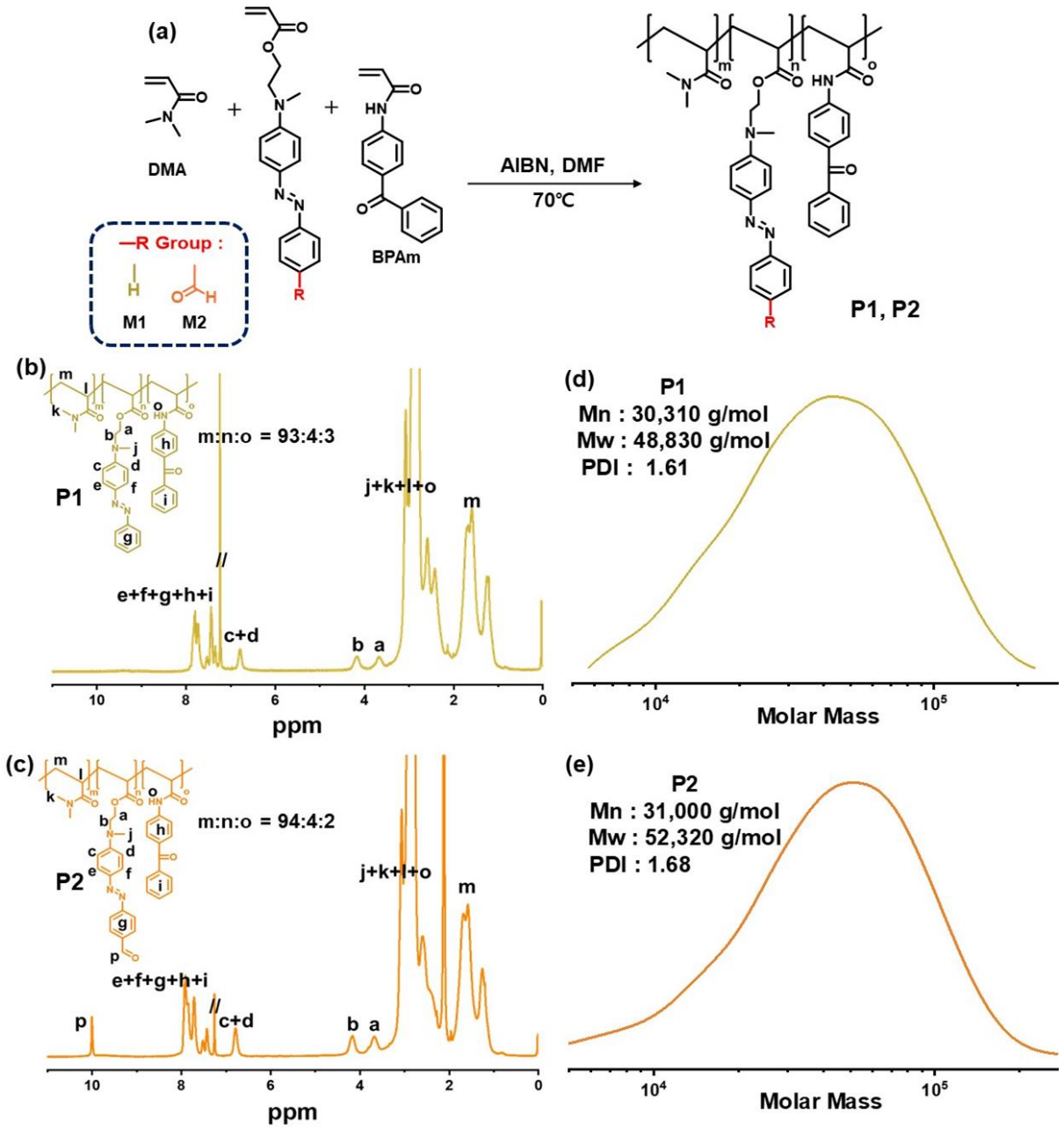

Figure 1. (a) Synthesis of p(DMA-*co*-M1-*co*-BPAm), P1 and p(DMA-*co*-M2-*co*-BPAm), P2; ^{1}H NMR spectra of (b) P1 and (c) P2 in $CDCl_3$; GPC trace of (d) P1 and (e) P2.

Demeton-S was synthesized through the chemical reaction between 2-(ethylthio)ethanethiol and diethyl chlorophosphate (Figures S1 and S2). It is widely acknowledged that certain metal cations, such as Au (III), form complexes with V-type nerve agents.10 Two chromophores (M1 and M2) were synthesized based on azobenzene, which exhibit binding affinity toward Au (III) ions. They were designed to explore the influence of variance in electron-withdrawing groups on the accurate identification of Au (III) and demeton-S, wherein M1 featured a hydrogen group while M2 contained an aldehyde group as a pendant. Briefly, M1 and M2 were obtained through the diazotization of 2-(methyl(phenyl)amino)ethyl acrylate and aminobenzene or 4-aminobenzaldehyde, respectively (Figure S3). The successful synthesis of M1 and M2 was confirmed using 1H NMR spectroscopy (Figure S4).

Figure 1a depicts the process of synthesizing terpolymers p(DMA-co-M1-co-BPAm), P1 and p(DMA-co-M2-co-BPAm), P2, which are utilized for the sequential colorimetric identification of Au (III) and demeton-S. P1 and P2 were obtained via FRP of DMA as the water-soluble unit, M1 or M2 as the Au (III) coordinating site as well as signaling unit, and BPAm as the film-anchoring unit. The copolymerization was performed in DMF using AIBN as an initiator at 70°C under argon atmosphere. The initial feed ratio of [DMA]:[M1 or M2]:[BPAm] was 94:4:2. After 12 h, the polymerization was terminated, and the reaction mixture was precipitated in cold ether and dried in a vacuum oven to yield P1 and P2. The synthesized P1 and P2 were characterized by 1H NMR. The determination of the ultimate feed ratios was accomplished through a comparative analysis of the relative integrated regions of each monomer component in 1H NMR spectra. The integrated areas of P1 and P2 were calculated using the peaks at 3.40–2.67 ppm for the dimethyl N-(CH3)2 protons of DMA, the aromatic protons of M1 (for P1) at 7.95–6.60 ppm, the aldehyde proton of M2 (for P2) at 10.0 ppm, and BPAm at 7.95–6.60 ppm (Figures 1b and 1c). The final feed ratios of [DMA]:[M1 or M2]:[BPAm] were 93:4:3 and 94:4:2 for P1 and P2, respectively, which were almost similar to the initial feed ratios. The number average molecular weight (Mn) and polydispersity index (PDI) of P1 were 48,830 Da and 1.61, respectively (Figure 1d). The Mn and PDI of P2 were 52,320 Da and 1.68, respectively (Figure 1e).

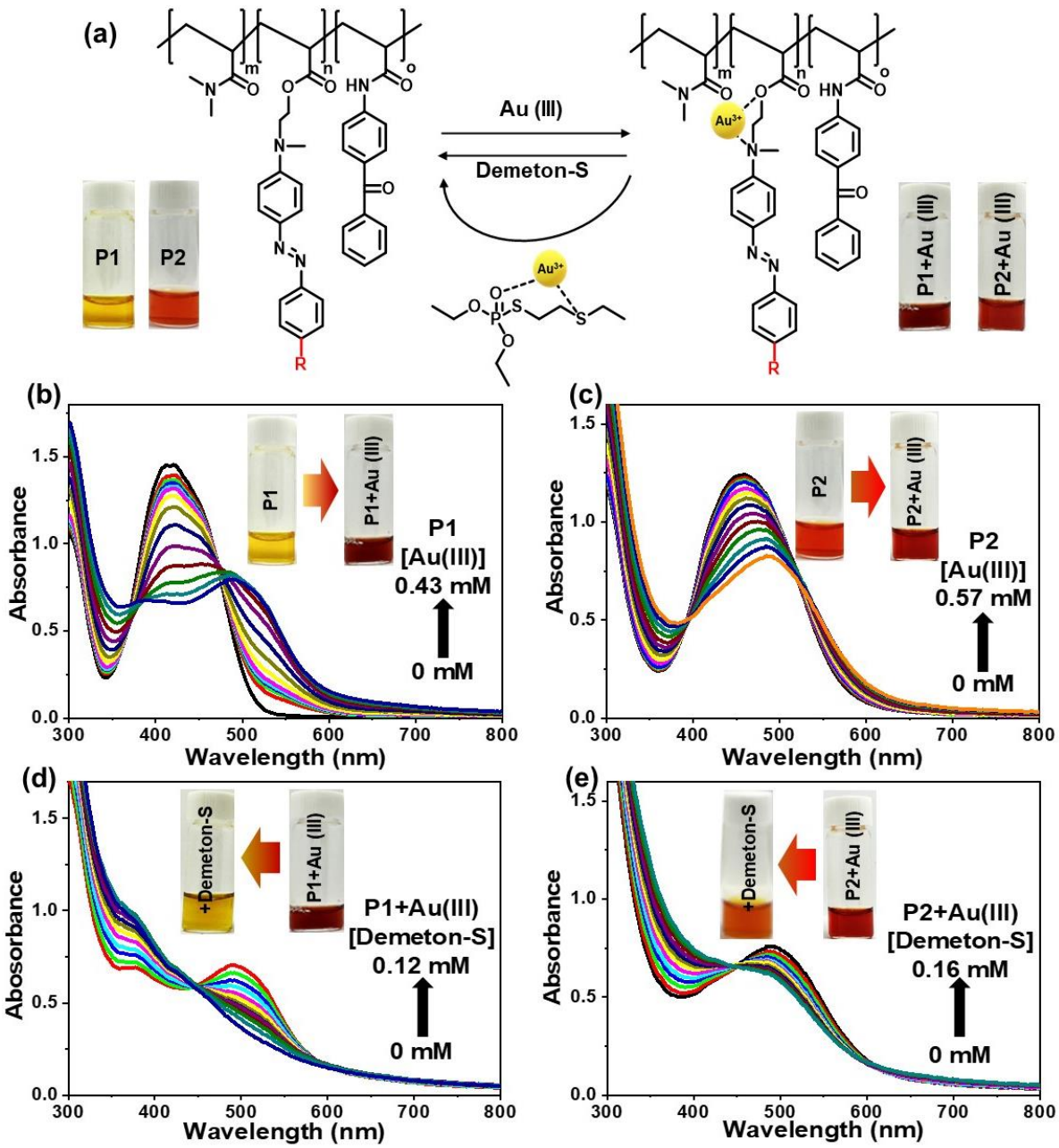

Figure 2. (a) Schematic diagram of Au (III) and demeton-S consecutive colorimetric detection in water (pH 7.4) at 25ºC and 60 % relative humidity using P1 and P2 (solution); UV–vis absorption spectra of (b) P1 (74.7 µM probe units; based on 4 % incorporation of M1). (c) P2 (71.6 µM probe units; based on 4 % incorporation of M2) with varying Au (III) concentration in water, inset: photographic images depicting the color changes upon the addition of Au (III) 0.43 mM (in P1) and 0.57 mM (in P2); UV–vis absorption spectra of (d) P1 + Au (III). (e) P2 + Au (III) with varying demeton-S concentration in water, inset: photographic images showing the color changes upon addition of demeton-S up to 0.12 mM (in P1 + Au (III)) and 0.16 mM (P2+Au (III)).

The consecutive detection of Au (III) and demeton-S using P1 and P2 was achieved by coordination with Au (III), followed by a simple displacement mechanism in which the demeton-S acts as a bidentate ligand toward Au (III) (Figure 2a). Au (III) coordination to the polymers was monitored using UV–vis absorption spectroscopy. The maximum absorption wavelength of P1 in water exhibited a progressive redshift from 417 to 495 nm with an increasing concentration of Au (III) up to 0.43 mM (Figure 2b). In case of P2, the absorption maximum gradually shifted toward longer wavelengths (from 455 to 495 nm) as the concentration of Au (III) increased up to 0.57 mM (Figure 2c). As shown in the photographic images inserted in Figures 2b and 2c, the aqueous solution of P1 and P2 changes color from yellow and orange to dark red, respectively, indicating the formation of metal–ligand complexes. The limit of detection (LOD) of P1 was 0.013 mM, obtained by calculating the linear relation between A_{495}/A_{417} and Au (III) (Figure S5a). The LOD of P2 was 0.037 mM, obtained by calculating the linear relation between $\Delta\lambda_{max}$ and Au (III) (Figure S5b). P1 and P2 exhibited good selectivity for Au (III) ions, as already reported in our previous paper. The increased electron-withdrawing nature of P2 results in the induction of an intramolecular charge transfer (ICT) effect, directing electrons toward the aldehyde compared to P1. Consequently, the binding of P2 to Au (III) is comparatively less responsive and slower than P1 and exhibits a higher LOD.

After the Au (III) coordination to the polymers, P1 + Au (III) and P2 + Au (III) solutions were employed as receptor solutions for the subsequent detection of demeton-S. The P1 + Au (III) solution revealed that the maximum absorption wavelength shifted from 495 to 417 nm as the concentration of demeton-S increases from 0 to 0.12 mM (Figure 2d). In the case of P2 + Au (III), the wavelength was shifted from 496 to 457 nm as the concentration of demeton-S progressively increased up to 0.16 mM (Figure 2e). As shown in the inset of Figures 2d and 2e, P1 + Au (III) and P2 + Au (III) solutions exhibited a noticeable color change from dark red to the original colors of the polymers, yellow and orange, respectively. The displacement of Au (III) by demeton-S causes P1 and P2 to revert to their original forms. The LOD values for demeton-S detection using P1 + Au (III) and P2 + Au (III) were calculated to be 0.004 and 0.006 mM, respectively (Figures S5c and S5d). The sensitivity of P2 + Au (III) is comparatively lower than that of P1 + Au (III) due to the presence of an aldehyde group, which slows down the displacement reaction.

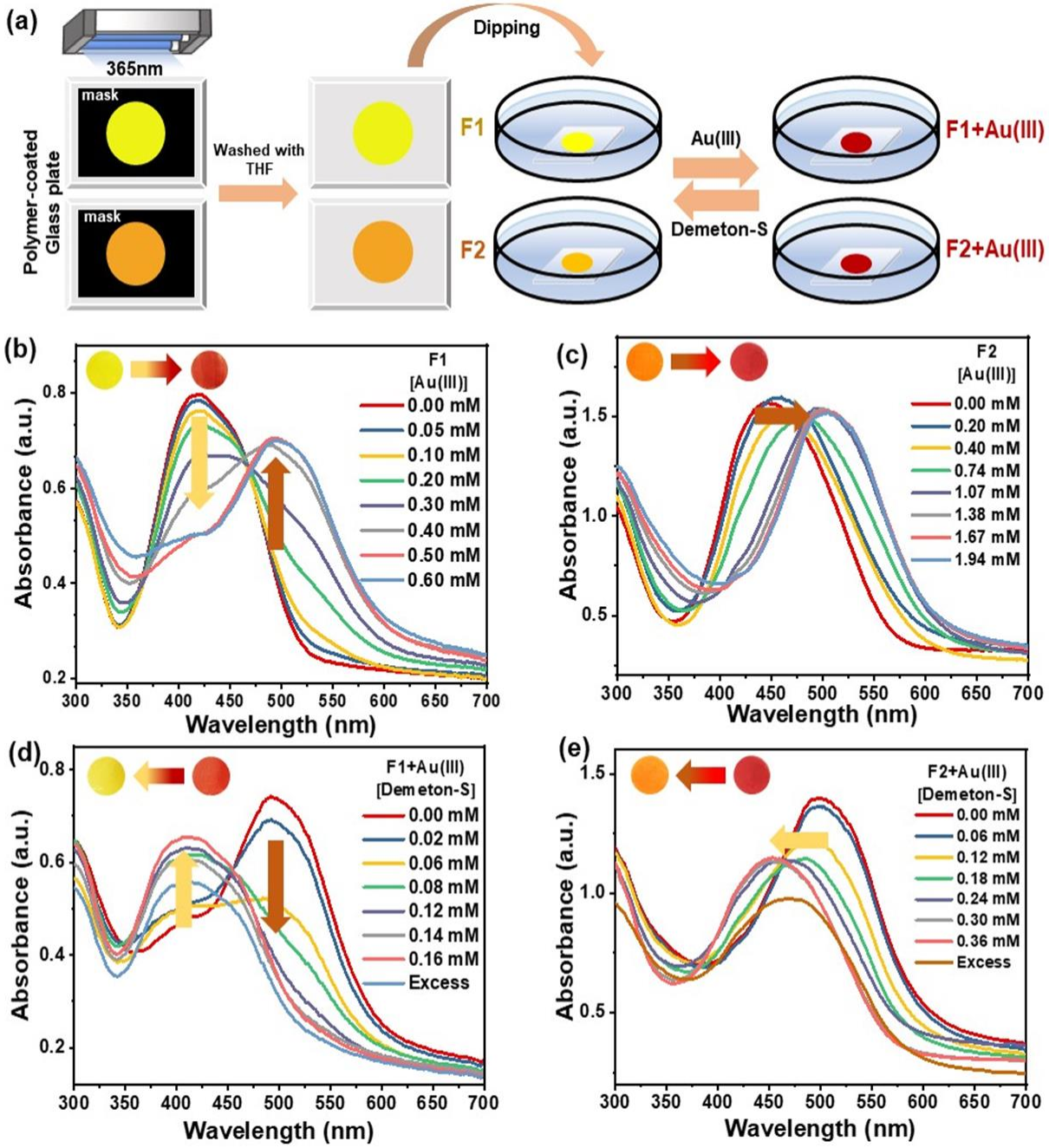

Figure 3. (a) Schematic illustration of the fabrication procedure of F1 and F2, followed by the consecutive detection of Au (III) and demeton-S in water (pH 7.4) at 25ºC and 70 % relative humidity; UV–vis absorption of (b) F1 and (c) F2 with varying amounts of Au (III) in water; UV–vis absorption of (d) F1 + Au (III) and (e) F2 + Au (III) with varying amounts of demeton-S in water.

The detection capability of a solution is constrained by several factors, including the challenges associated with the reduction of gold ions to metal and the stability of the Au (III)–demeton-S complex (Figure S6). Thus, the implementation of a heterogeneous film surface could potentially serve as a feasible resolution to the aforementioned problem. The solutions of P1 and P2 dissolved in propanol were spin-coated to a glass slide, followed by UV light (365 nm) irradiation for 5 min to immobilize the polymers to the glass surface to yield F1 and F2, respectively.38 Subsequently, F1 and F2 were washed thoroughly with THF and dried in a vacuum oven overnight before use (Figure 3a).

The UV–vis spectra of F1 and F2 were analyzed. The colorimetric detection of Au (III) using F1 and F2 was subsequently validated with the polymeric solution data. The observed shift in the maximum absorption wavelength of F1 from 417 to 495 nm occurs as the concentration of Au (III) reaches 0.60 mM (Figure 3b). The alteration in the color of F1 was visually perceived, transitioning from yellow to deep red (Figure 3b inset). Figure 3c shows that the maximum absorption wavelength of F2 undergoes a redshift from 455 to 495 nm as the color transitioned from orange to red due to ICT enhancement. The LODs for the detection of Au (III) using F1 and F2 were determined to be 0.072 and 0.14 mM, respectively (Figures S7a and S7b).

The Au (III) coordinated films, F1 + Au (III) and F2 + Au (III), were employed for the investigation of demeton-S detection by displacement mechanism. F1 + Au (III) exhibited a complete shift in the absorption maximum wavelength to the original wavelength around 415 nm as the concentration of demeton-S gradually increased (up to 0.16 mM) (Figure 3d). Furthermore, the absorption maximum wavelength of F2 + Au (III) returned to the original position when the concentration of demeton-S increased up to 0.36 mM (Figure 3e). The LOD values of demeton-S by F1 + Au (III) and F2 + Au (III) were calculated to be 0.021 and 0.052 mM, respectively (Figures S7c and S7d). The LOD for demeton-S detection by both films were found to be far lower than the deadly dose of VX in humans (Table S1). This finding enhances the system's utility and desirability for real-time applications.

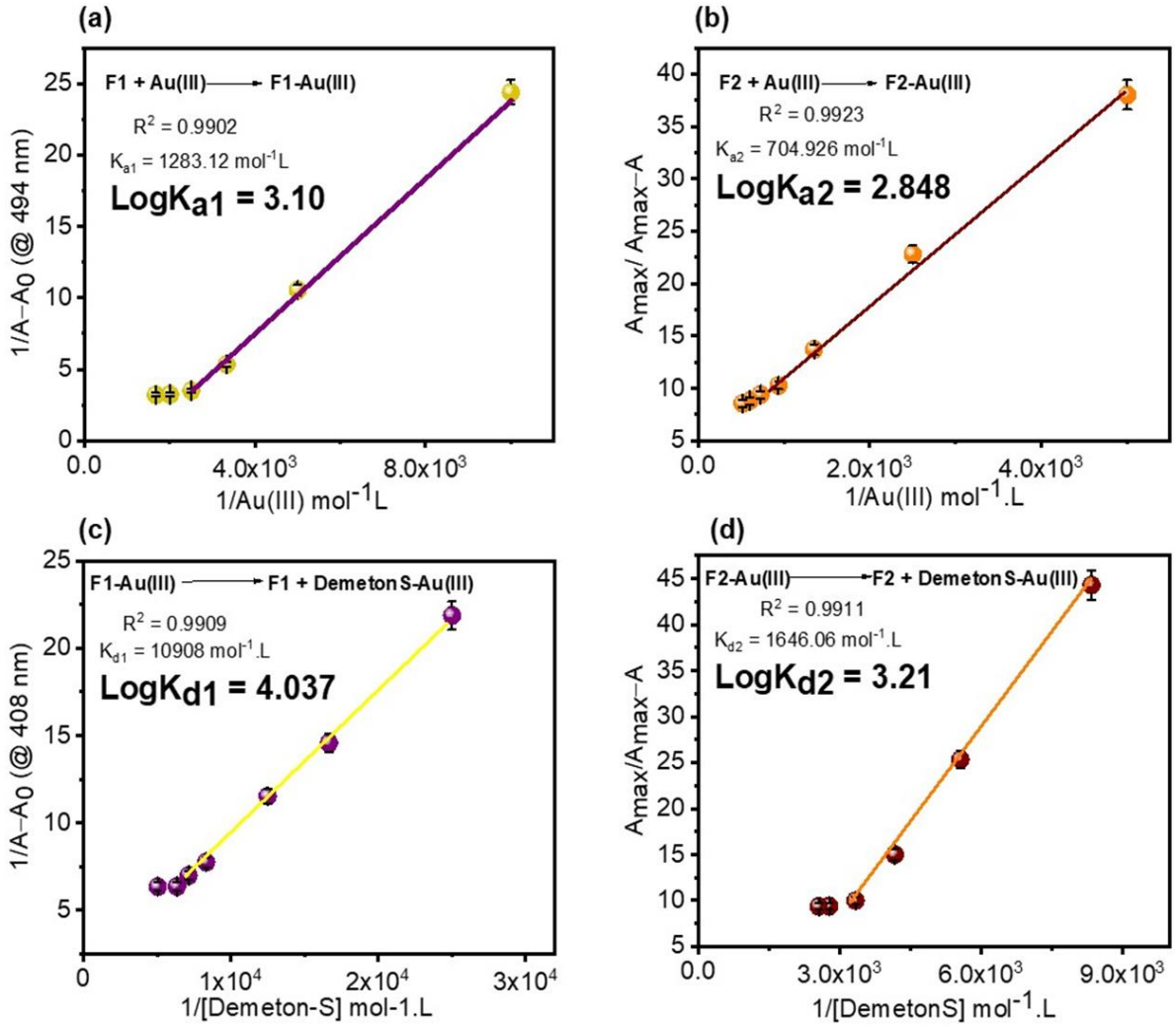

Figure 4. Association constant of binding Au (III) by (a) F1 (b) F2 and displacement constant by demeton-S of (c) F1+Au (III) (d) F2+Au (III).

The determination of the sensing mechanism involved the calculation of the association constant (Ka) between Au (III) ions and F1 or F2. This was achieved through the implementation of UV-vis titration experiments employing the Benesi-Hildebrand equation. The logarithms of the equilibrium constants (log Ka) for the production of the 1:1 complex between F1 and Au (III), and between F2 and Au (III) were determined to be 3.10±0.2 and 2.84±0.4, respectively (Figure 4a and 4b). In contrast, the logarithm (referred to as log Kd) of the displacement reaction of Au (III) from F1-Au (III) and F2-Au (III) by demeton-S was also determined to be 4.03±0.8 and 3.21±0.5, respectively (Figure 4c and 4d). The findings of these tests indicate that Au(III) exhibited a higher affinity for demeton-S compared to polymeric film F1 or F2, which aligns with the hypothesized sensing mechanism (Table S2).

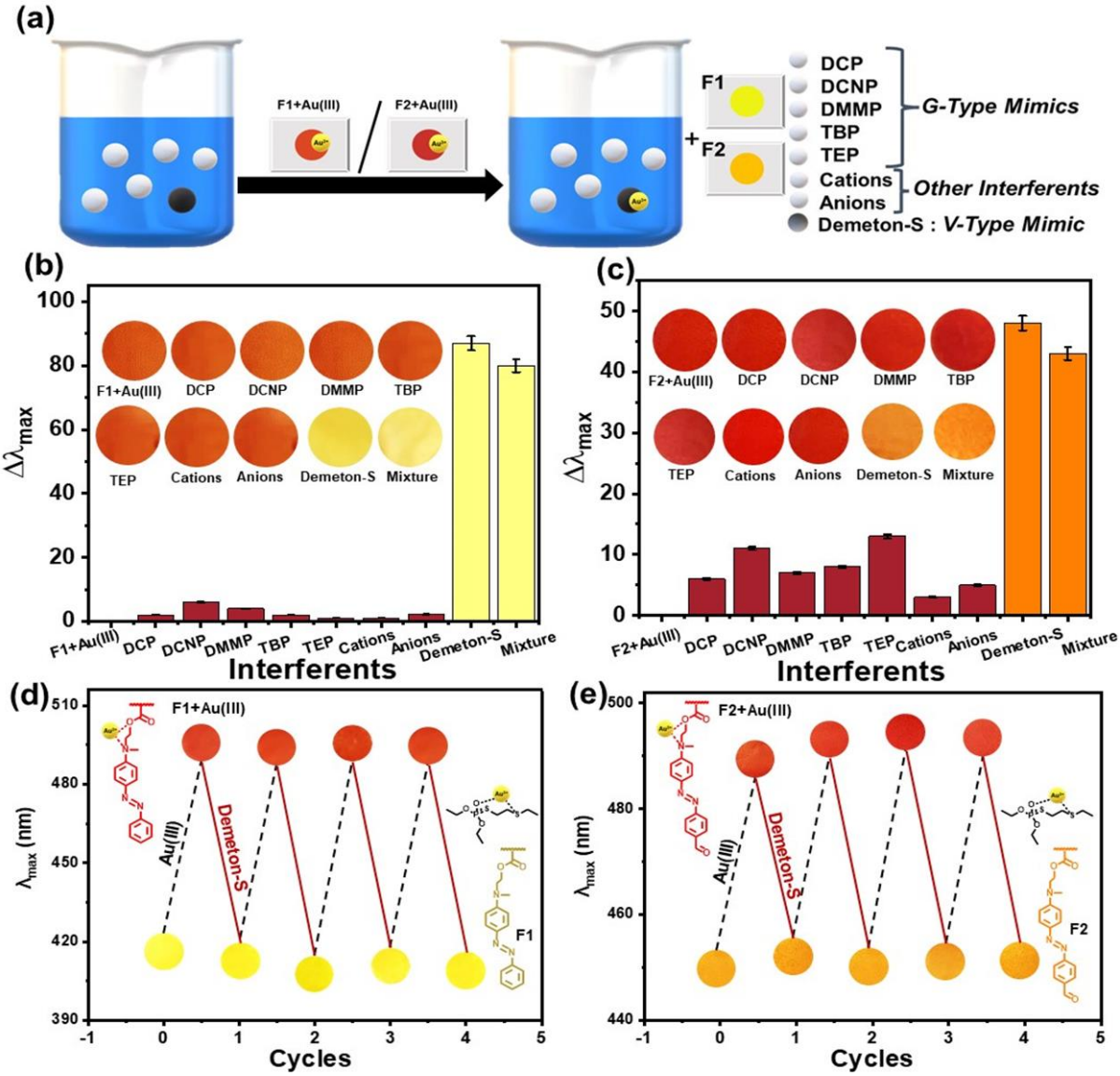

Figure 5. (a) Schematic representation of the selective V-type nerve agent detection in water (pH 7.4) at 25ºC and 60 % relative humidity in the presence of various G-type nerve agent mimics and other interferents using F1 + Au (III) or F2 + Au (III); Selectivity bar diagram and photographs in the presence of DCP, DCNP, DMMP, TBP, TEP, cations, anions, demeton-S, and mixture (DCP + DCNP + DMMP + TBP + TEP + cations + anions + demeton-S) using (b) F1 + Au (III) (0.16 mM interferents) and (c) F2 + Au(III) (0.36 mM interferents); Reversibility and cyclic stability of (d) F1 and (e) F2 for the successive detection of Au (III) and demeton-S in water up to four cycles.

To evaluate the selectivity of demeton-S over the most probable interferents such as, G-type nerve agent mimic, cations, and anions the films of F1 + Au (III) and F2 + Au (III) were analyzed using UV–vis spectroscopy and naked eye observation. The present analysis was performed in the presence of G-type nerve agent mimics and a variety of organophosphorus compounds, namely phosphoryl, DCP, DCBP, DMMP, TBP, TEP and cation, anions namely Na+, K+, Mg2+, Ca2+, SO2-, HCO3-, PO43- (Figure 5a). Figures 5b and 5c illustrate the changes in the absorption maxima ($\Delta\lambda max$) of the films after being subjected to various interferents. F1 + Au (III) and F2 + Au (III) did not exhibit any noticeable changes in the absorption maxima when other interferents were present. Nevertheless, it was observed that only demeton-S exhibited a discernible alteration in color, thereby suggesting the advantageous selectivity of the film toward the V-type mimic (Figure S8 and S9).

The reusability of F1 and F2 in consecutively detecting Au (III) and demeton-S for multiple cycles has been determined. This was achieved by sequentially introducing the films into solutions containing Au (III) ions and demeton-S. The binding of Au (III) to F1and F2 resulted in a red shift in their wavelengths, which were subsequently blue-shifted upon exposure to demeton-S. The observed maximum absorption wavelength of F1 exhibited a shift from 418 to 495 nm upon addition of 0.7 mM Au (III), followed by a subsequent return to 413 nm upon addition of 0.16 mM demeton-S (Figure 5d). Similarly, the maximum absorption wavelength of F2 displayed a shift from 450 to 490 nm in the presence of 1.95 mM Au (III), with a subsequent return to 453 nm in the presence of 0.36 mM demeton-S (Figure 5e). The aforementioned procedure was effectively replicated for a total of four iterations for each film, demonstrating the stability of the film. The findings of this study validate the suitability of polymeric films for reversible and repeatable detection, thus highlighting the potential of these reusable materials for practical applications.

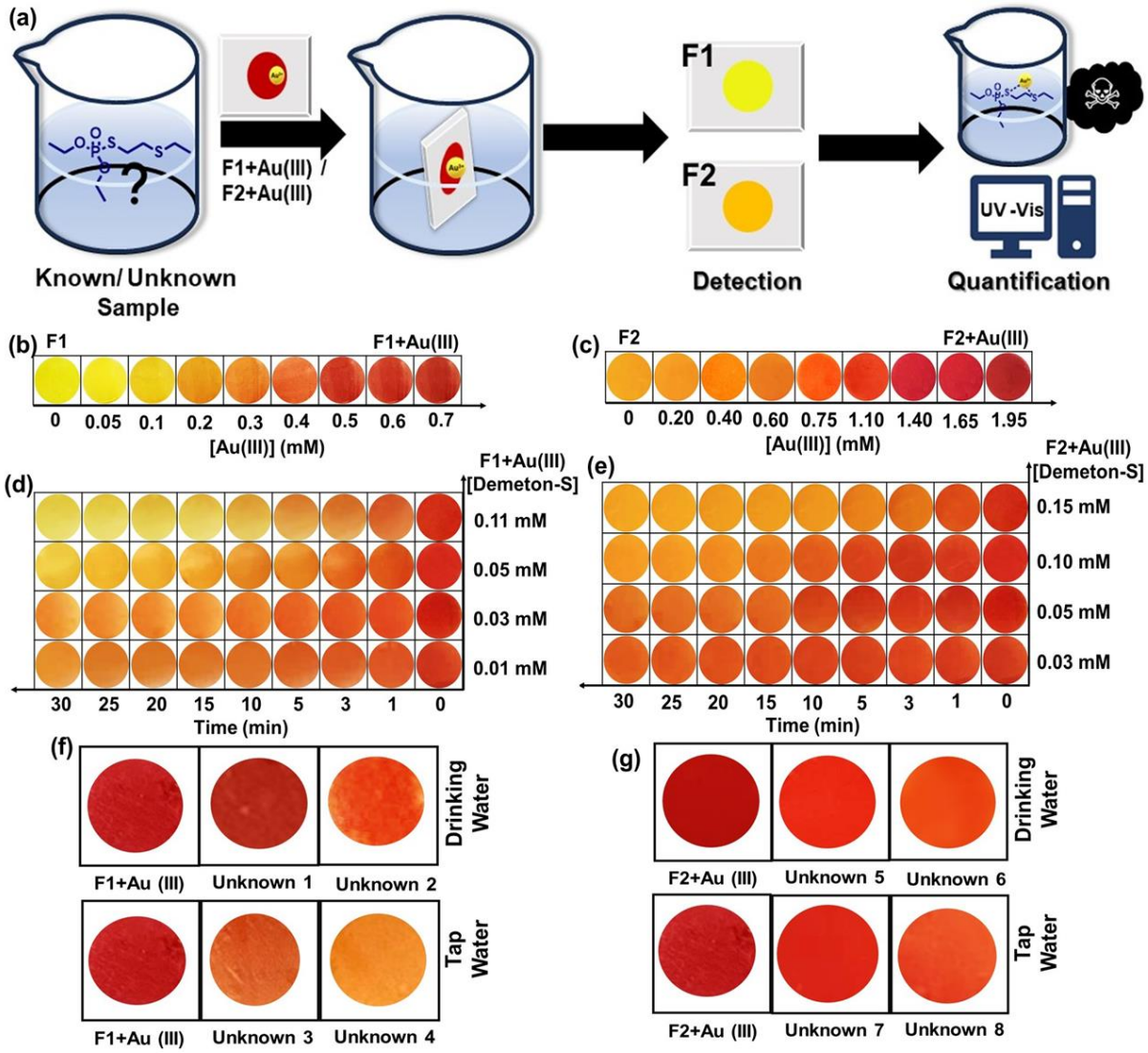

Figure 6. (a) Schematic illustration of the colorimetric detection of demeton-S in known and unknown water samples at 25ºC and 60 % relative humidity using F1 + Au (III) or F2 + Au (III); Photographs of color-differentiation map depicting the detection of Au (III) using (b) F1 and (c) F2 to yield F1 + Au (III) and F2 + Au (III); Color-differentiation map showing the relation between the concentration of demeton-S and the detection time of (d) F1 + Au (III) and (e) F2 + Au (III); Photographs of polymeric films after detection and quantification of demeton-S in unknown samples of drinking and tap water by (f) F1 +Au (III) and (g) F2 +Au (III).

Following the verification of the sensitivity, selectivity and reusability of the film, the efficacy of the film detection platform was demonstrated in a practical scenario. The detection of demeton-S in real-time and across different media in the field is a crucial aspect of the research in sensing, given their persistence in actual war sites and lethal nature upon exposure. First, an attempt was made to identify the presence of demeton-S in contaminated water using Au (III) coordinated films F1 or F2, based on their color change (Figures 6a and S10). Different concentrations of Au (III) were introduced, and the resulting changes in appearance were observed after 1 min. The alteration in color observed in the films is attributed to the coordination between Au (III) and the film, resulting in a shift from yellow to red for F1 and orange to dark red for F2 (Figures 6b and 6c).

Following the observations of Au (III) binding to the film surface, further investigation was performed for tracing demeton-S in the contaminated water. To examine the detection of demeton-S using F1 + Au (III) or F2 + Au (III), different concentrations of demeton-S were introduced, and the color change was observed. In addition, we aimed to establish a correlation between the duration of detection and the demeton-S concentration, given its highly hazardous nature in residual state. This necessitates the need for precise detection thresholds and rapid detection capabilities in the event of potential exposure. The time profile for detecting different concentrations of demeton-S was measured using F1 + Au (III) and represented using a color-differentiation map, as shown in Figure 6d. The study revealed that the duration for detecting a concentration of 0.11 mM of demeton-S is less than a 1 min. Furthermore, the detection time increased with decreasing demeton-S concentration (0.01, 0.03, and 0.05 mM). Nevertheless, when the concentration dropped below 0.05 mM, no discernible alteration in color even after an extended duration was observed. The implementation of demeton-S causes the reinstatement of the initial yellow color of the film. The time profile of F2 + Au (III) detection toward demeton-S at various concentrations is represented using a color-differentiation map (Figure 6e). The detection was observed for 0.15 mM demeton-S within 3 min. Moreover, the LOD for F2 + Au (III) (0.052 mM) was greater than that of F1 + Au (III). The contents of unknown samples in drinking and tap water were quantified using F1+ Au (III) and F2 + Au (III), utilizing the standard calibration curve obtained from a known sample experiment. The acquired results validate the system's capability to efficiently detect (Figure 6f and 6g) and quantify (Figure S11 and Table 1) demeton-S, even in the presence of competitive factors that are typically considered challenging.

Polymeric Film	Type	Sample Name	Added (mM)	Found (mM)*	Recovery (%)
F1+ Au (III)	Drinking Water	Unknown 1	0.04	0.038	95.0
		Unknown 2	0.10	0.098	98.0
	Tap Water	Unknown 3	0.10	0.097	97.0
		Unknown 4	0.20	0.200	100
F2+ Au (III)	Drinking Water	Unknown 5	0.07	0.067	95.7
		Unknown 6	0.10	0.098	98.0
	Tap Water	Unknown 7	0.07	0.069	98.5
		Unknown 8	0.10	0.099	99.0

Table 1: Quantification of demeton-S in various unknown water samples.

Polymeric Film	Type	Sample Name	Added (mM)	Found (mM)*	Recovery (%)
F1+ Au (III)	Drinking Water	Unknown 1	0.04	0.038	95.0
		Unknown 2	0.10	0.110	110.0
	Tap Water	Unknown 3	0.10	0.132	132.0
		Unknown 4	0.20	0.261	130.5
F2+ Au (III)	Drinking Water	Unknown 5	0.07	0.075	107.1
		Unknown 6	0.10	0.110	110.0
	Tap Water	Unknown 7	0.07	0.080	114.3
		Unknown 8	0.10	0.111	111.0

*An average of three replicate measurement

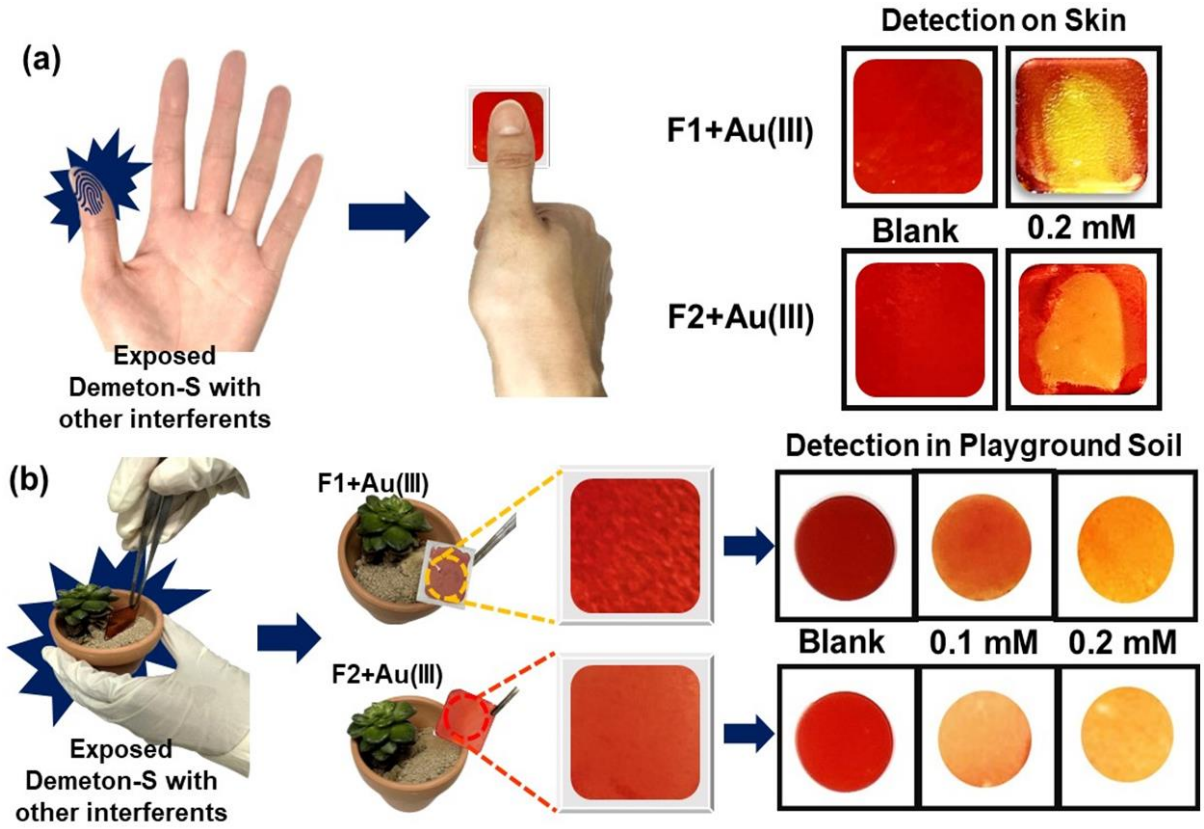

Figure 7. Practical application demonstrating detection of exposed demeton-S at 25ºC and 60 % relative humidity in presence of other interferents (a) on skin and (b) in playground soil by F1 + Au (III) and F2 + Au (III). [Blank: other interferents (No demeton-S)].

This study focused on investigating demeton-S detection in presence of other interferents on the skin. Upon contact with F1 + Au (III) or F2 + Au (III), clear fingerprints were immediately observed when fingers contaminated with demeton-S were exposed. Furthermore, no color change was observed when monitored with an exposed skin with only other interferents. But a color change to yellow was observed in the exposed portion of the fingerprint when treated with demeton-S in the case of F1 + Au (III), while a color change to orange was observed in the case of F2 + Au (III) (Figure 7a). The results obtained from the visualization of fingerprints demonstrated the feasibility of detecting demeton-S on the skin.

Moreover, the detection of demeton-S concealed within playground soil was assessed. In this experiment, demeton-S with other interferents (0.1 and 0.2 mM) was introduced into a pot culture and left undisturbed for a day. Upon interaction with demeton-S present on the uppermost layer of the soil, a rapid alteration in the coloration of the film was observed within 1 min (Figure S12). Notably, this color change occurred irrespective of any potential influence from the soil matrix or other chemical constituents present in the soil, as shown in Figure 7b. Specifically, the F1 + Au (III) film exhibited a transformation to dark yellow color, while the F2 + Au (III) film displayed a shift toward dark orange color. This phenomenon exhibits considerable promise for the detection and interpretation of real-world occurrences via a straightforward methodology.

Table S3 presents a comparative analysis of thin polymeric films and other previously reported techniques for detecting V-type nerve agent mimics. The comparison is based on factors such as the method employed, the medium used, the selectivity achieved, and the practical application. The current state of research mostly focuses on the detection by the identification of their degradation products.13 However, this approach lacks the necessary selectivity towards V-type agents when compared to G-type agents. There has been limited attention given to the detection of VX prior to its decomposition.[39] However, the majority of the detection has been carried out in mixed organic solvents. Furthermore, there is a dearth of practical applicability in terms of detecting across different media and quantifying. In contrast, the current colorimetric polymeric films have the capability to identify demeton-S, a VX mimic, using a metal displacement mechanism in diverse contaminated environments with a significantly higher level of selectivity over other interfering substances. Furthermore, the potential of quantifying demeton-S in unknown samples to assess their appropriateness for on-site measurements. This approach exhibits promise in the detection of V-type nerve toxin mimics, surpassing other previously described systems.

4. Conclusions

We successfully developed two colorimetric polymeric films to rapidly and sensitively detect demeton-S in contaminated environments. The strategic integration of a coordination site for Au (III) ions and azobenzene-based signaling structures with two different pendant-R groups allowed us to enhance the sensitivity of the film for demeton-S detection. The experimental results demonstrated that the coordination of the polymeric films with Au (III) caused a discernible color change, providing a reliable indication of the presence of demeton-S. Upon exposure to demeton-S, the displacement of Au (III) within the films resulted in the restoration of their original color, further verifying their efficiency as indicators for demeton-S detection. The difference in association and displacement constants of Au (III) towards polymeric films and demeton-S proves the mechanism. Notably, the polymeric films displayed remarkable selectivity toward demeton-S over G-type nerve agents, and other potential interferences. demonstrating their potential as specific VX detection tools. Moreover, the reusability of the film, facilitated by their reversibility during alternate exposure to Au (III) and demeton-S, adds practical value and economic feasibility to their implementation. The versatility of these polymeric films is evident as they exhibited remarkable practical capabilities in various affected regions, including water, soil, and skin. These films exhibited effectiveness in detecting and quantifying demeton-S in various stimulated water samples. The novelty of this work is based on the fact that the engineered colorimetric thin polymeric films have a high affinity for VX mimics over G-type agents and can be reused without any significant degradation, offering practical VX detection on-site measurements.

5. Supporting Information

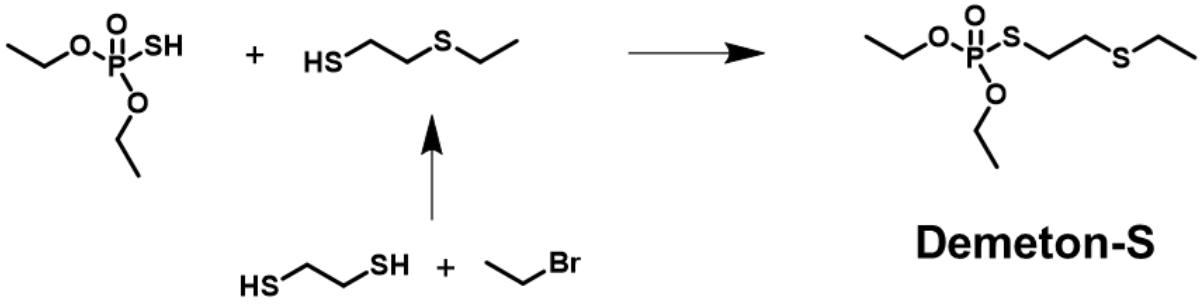

Figure S1. Synthesis of Demeton-S.

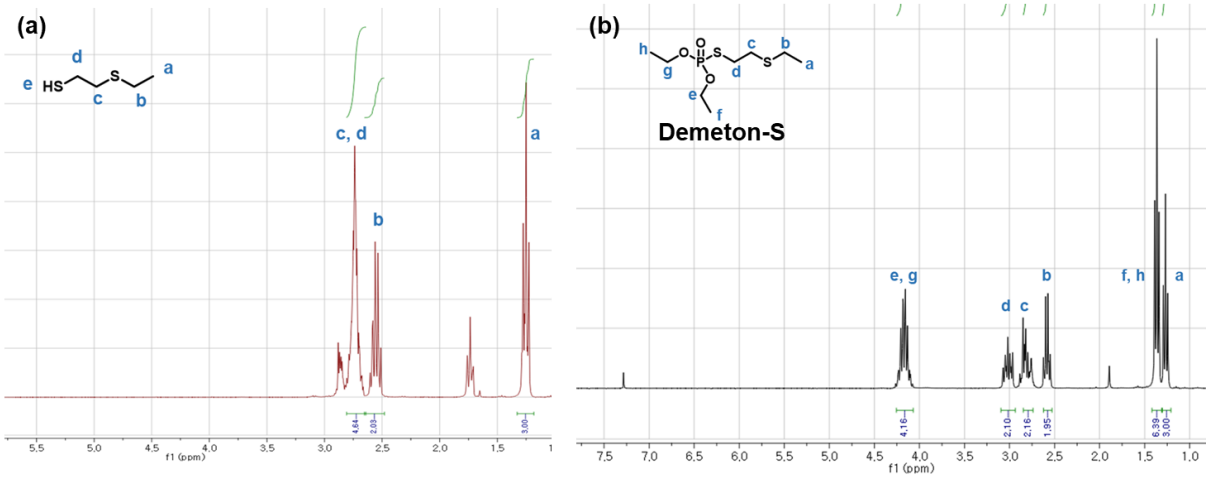

Figure S2. ^{1}H NMR characterization of (a) 2-(ethylthio)ethanethiol (b) Demeton-S.

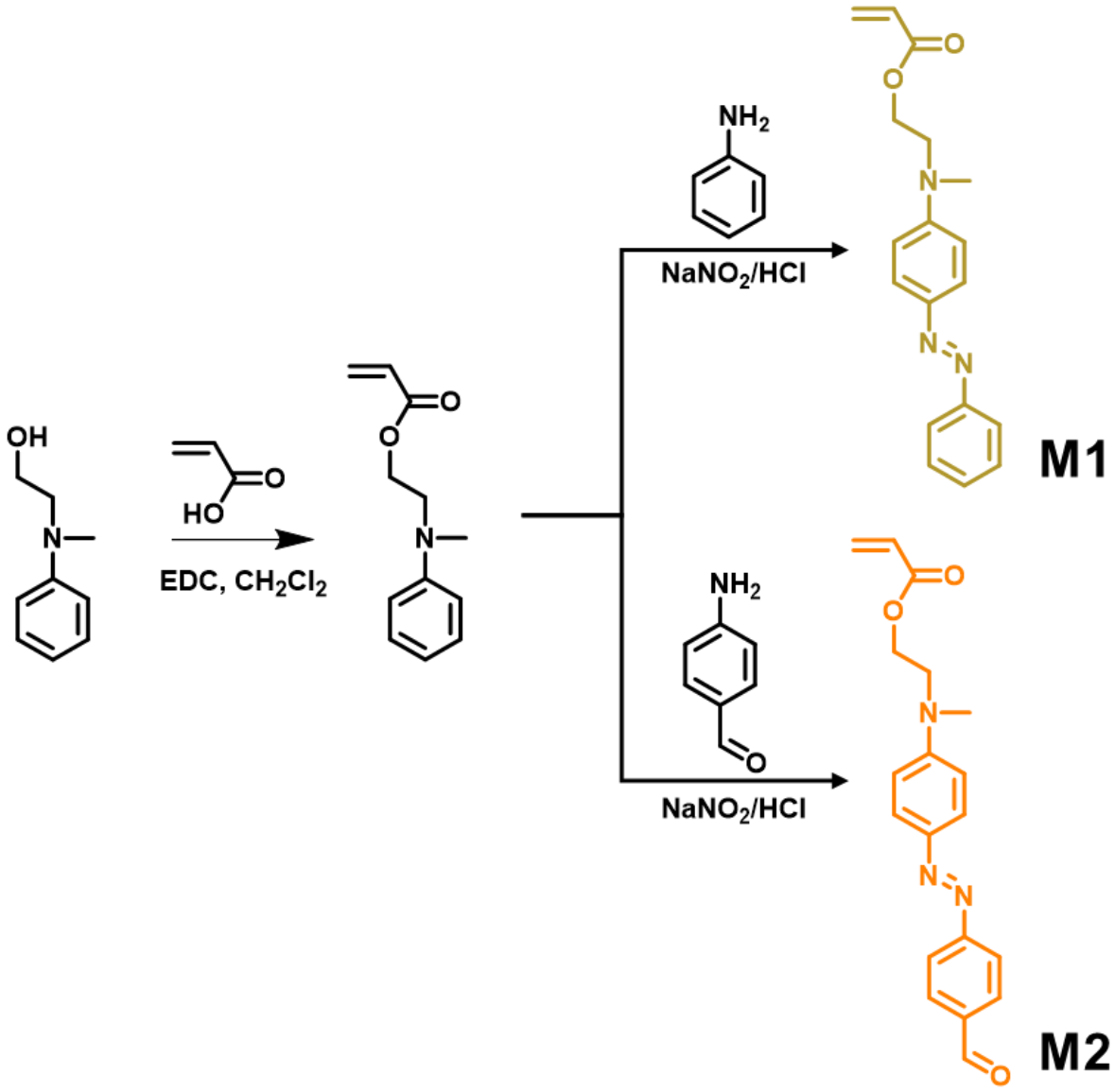

Figure S3. Synthesis of M1 and M2.

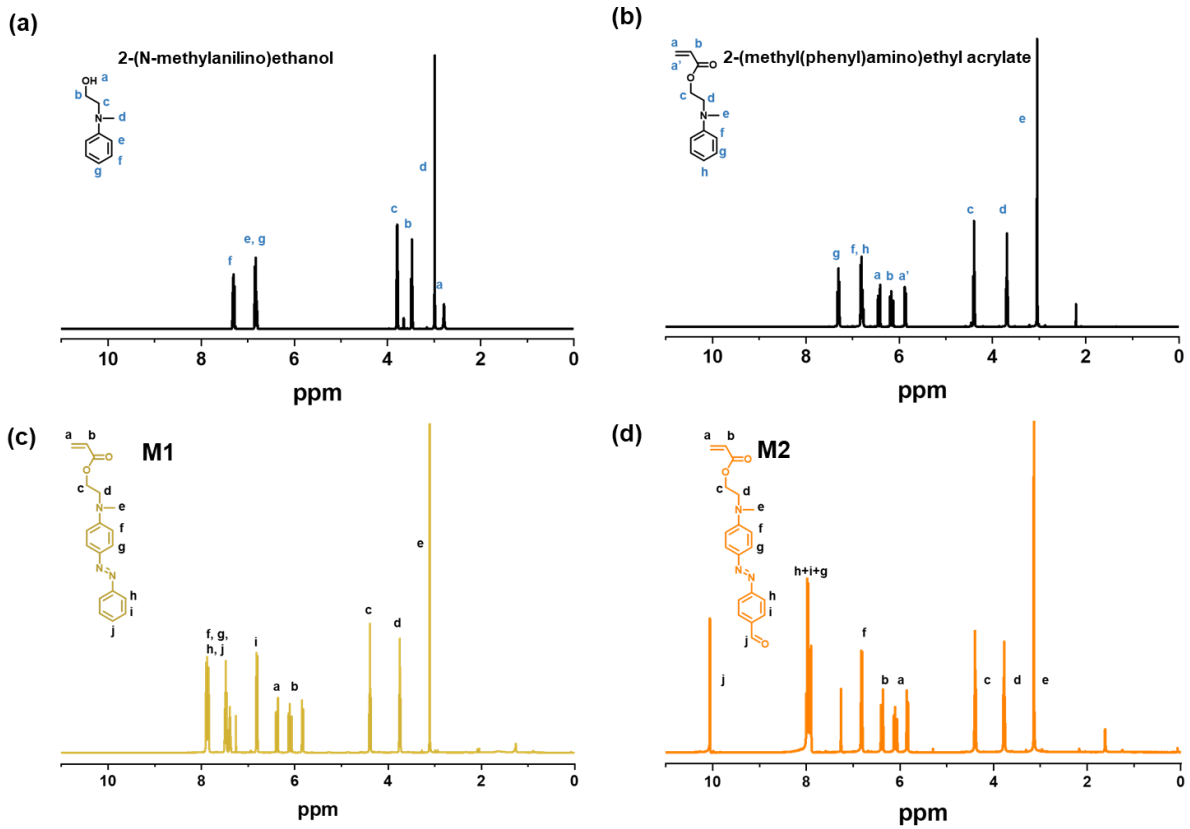

Figure S4. ^{1}H NMR characterization of (a)2-(N-methylanilino)ethanol

(b) 2-(methyl(phenyl)amino)ethyl acrylate (c) M1 (d) M2.

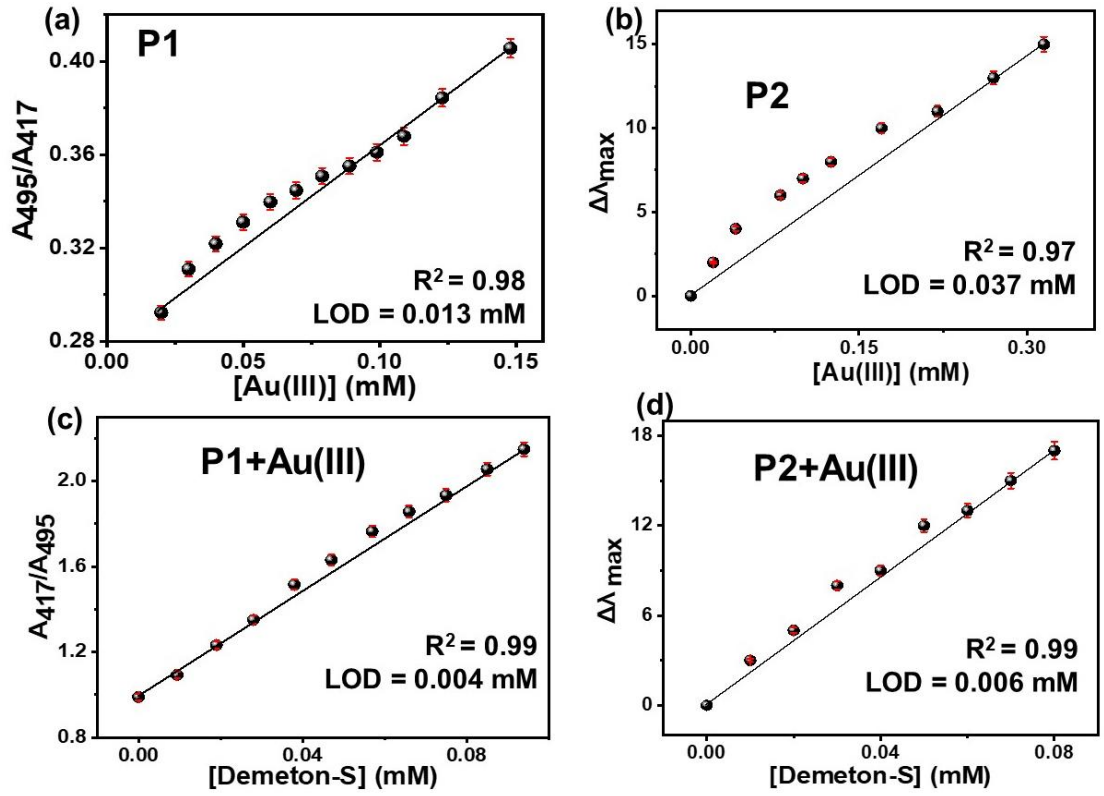

Figure S5. LOD of (a) P1 (b) P2 (c) P1+Au (III) (d) P2+Au (III).

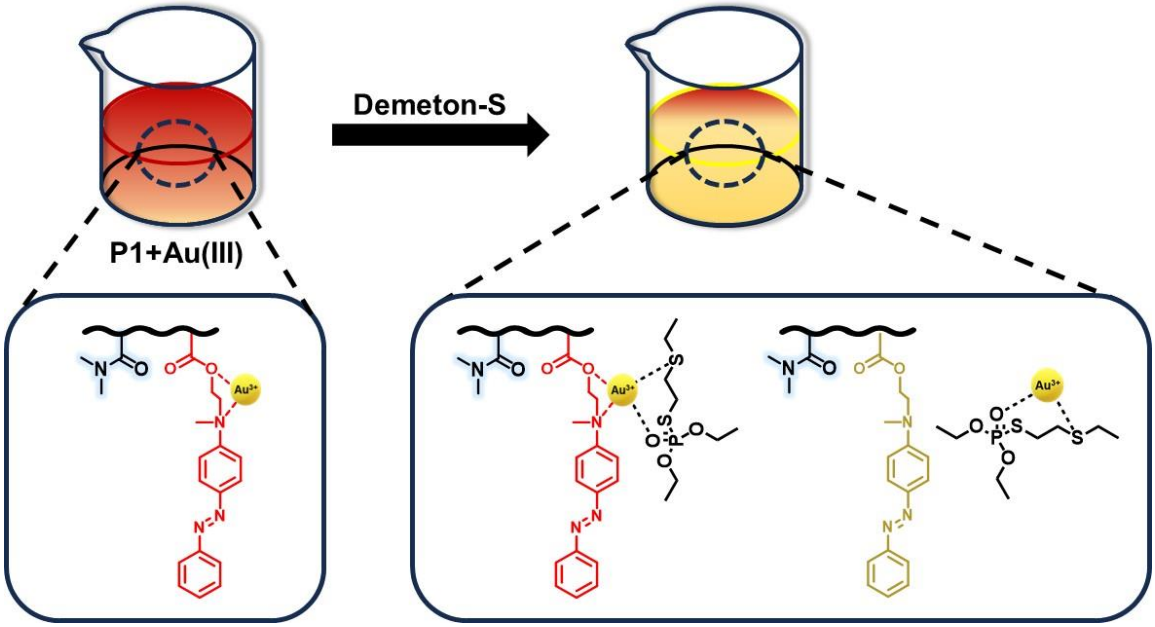

Figure S6. Mechanism of demeton-S detection in water by P1 + Au (III) solution.

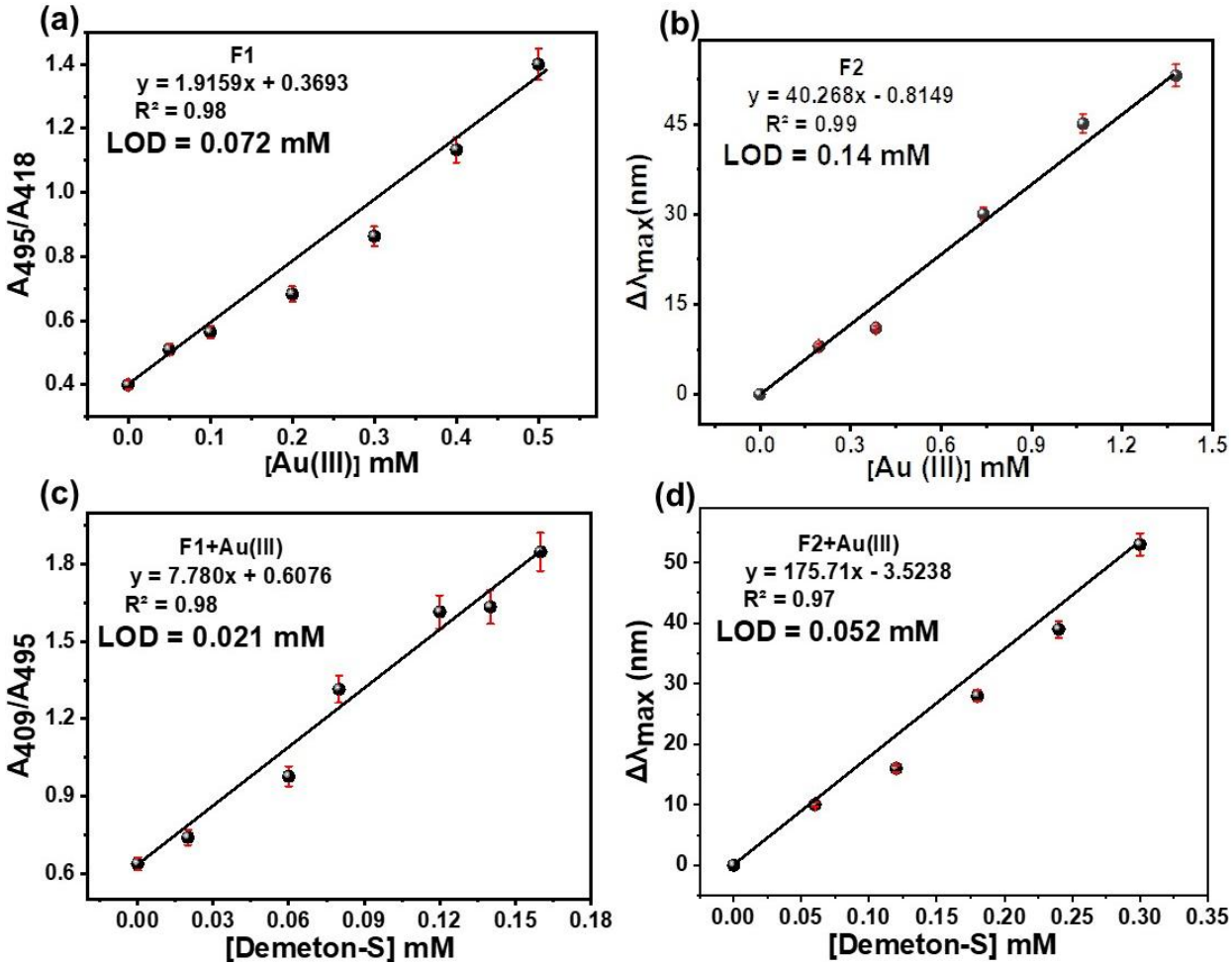

Figure S7. LOD of (a) F1 (b) F2 (c) F1+Au (III) (d) F2+Au (III).

Table S1: Comparison of Toxicity and limit of detection (LOD).

Oral VX LD_{50} (mg/ Individual)	Limit of Detection (mg/ml): UV-vis method (linear regression curve)		Limit of Detection (mg/ml): visual method	
	F1+Au (III)	F2+Au (III)	F1+Au (III)	F2+Au (III)
3-10	0.00542	0.0134	0.0154	0.0309

$$F1 + Au(III) \rightarrow F1 - Au(III) \ldots\ldots\ldots\ldots \boldsymbol{Ka1}$$

$$F1 - Au(III) + DemetonS \rightarrow F1 + DemetonS - Au(III) \ldots\ldots\ldots\ldots \boldsymbol{Kd1}$$

$$F2 + Au(III) \rightarrow F2 - Au(III) \ldots\ldots\ldots\ldots \boldsymbol{Ka2}$$

$$F2 - Au(III) + DemetonS \rightarrow F2 + DemetonS - Au(III) \ldots\ldots\ldots\ldots \boldsymbol{Kd2}$$

Table S2: Association (K_a) and Displacement (K_d) Constants of Au (III) binding by F1 or F2 followed by demeton-S.

Phenomenon	Log K
F1 → F1-Au(III)	Log K_{a1} : 3.10±0.2
F1-Au(III) → DemetonS-Au(III)	Log K_{d1} : 4.03±0.8
F2 → F2-Au(III)	Log K_{a2} : 2.84±0.4
F1-Au(III) → DemetonS-Au(III)	Log K_{d2} : 3.21±0.5

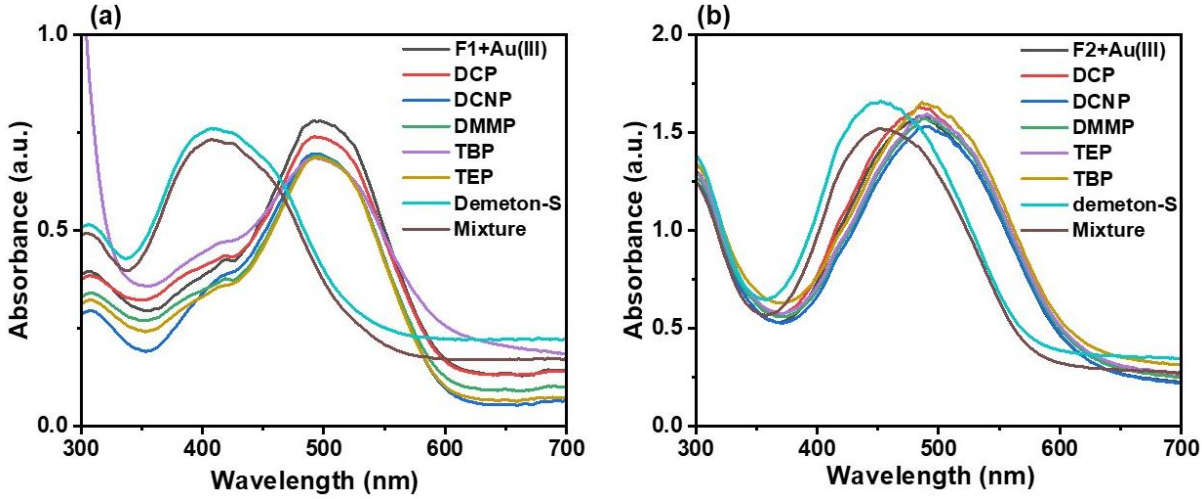

Figure S8. Selectivity towards V type over G type nerve agents by (a) F1 +Au (III) and (b) F2 + Au (III).

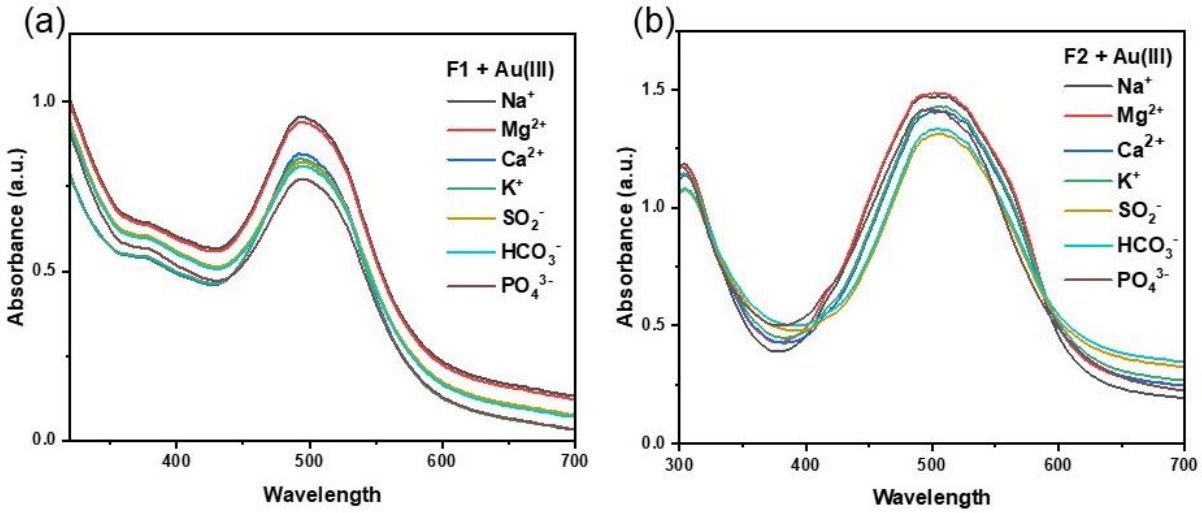

Figure S9. Selectivity towards V type over other interferents by (a) F1 +Au (III) and (b) F2 + Au (III).

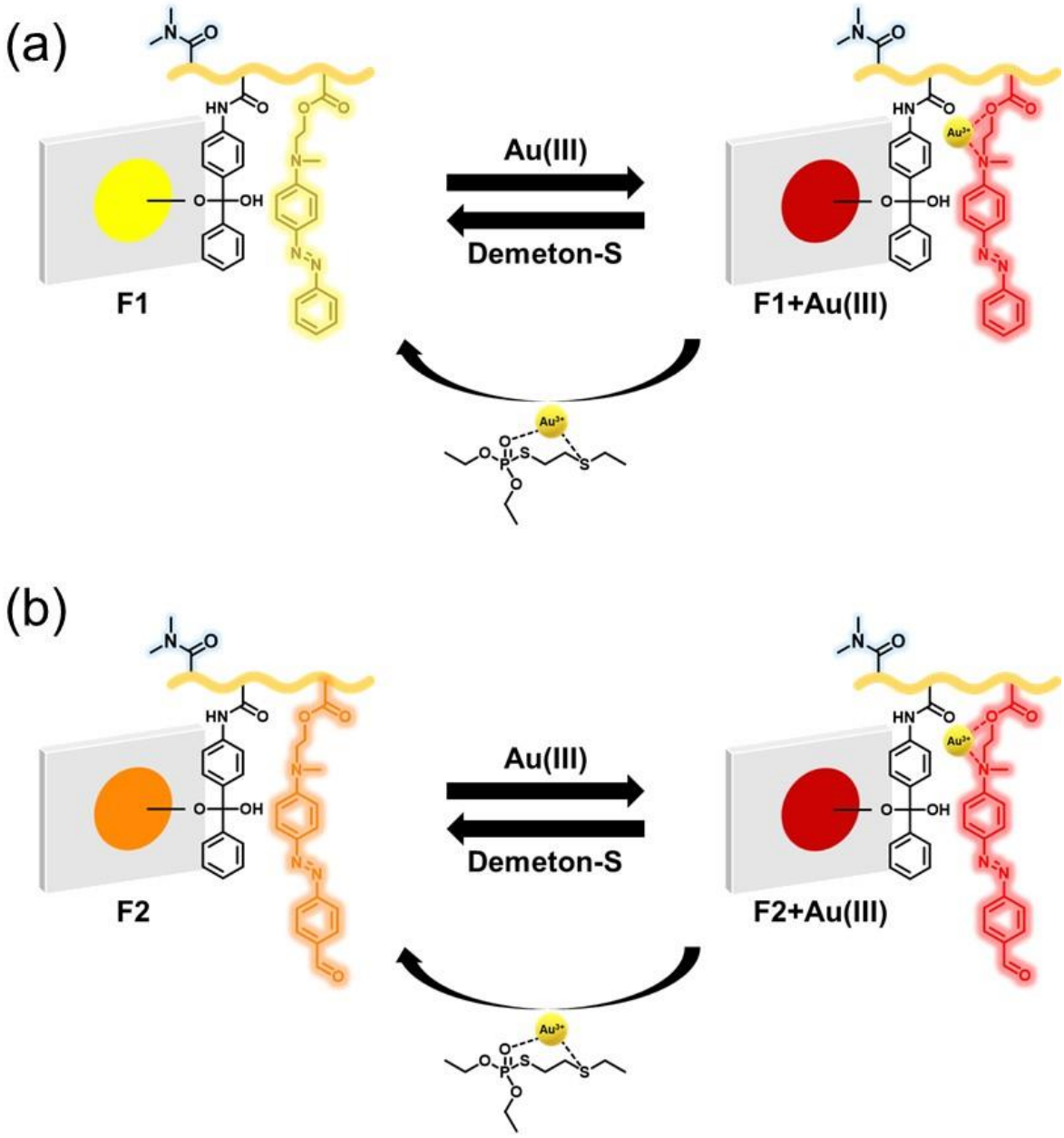

Figure S10. Mechanism of Au (III) and demeton-S detection in water by (a) F1 (b) F2.

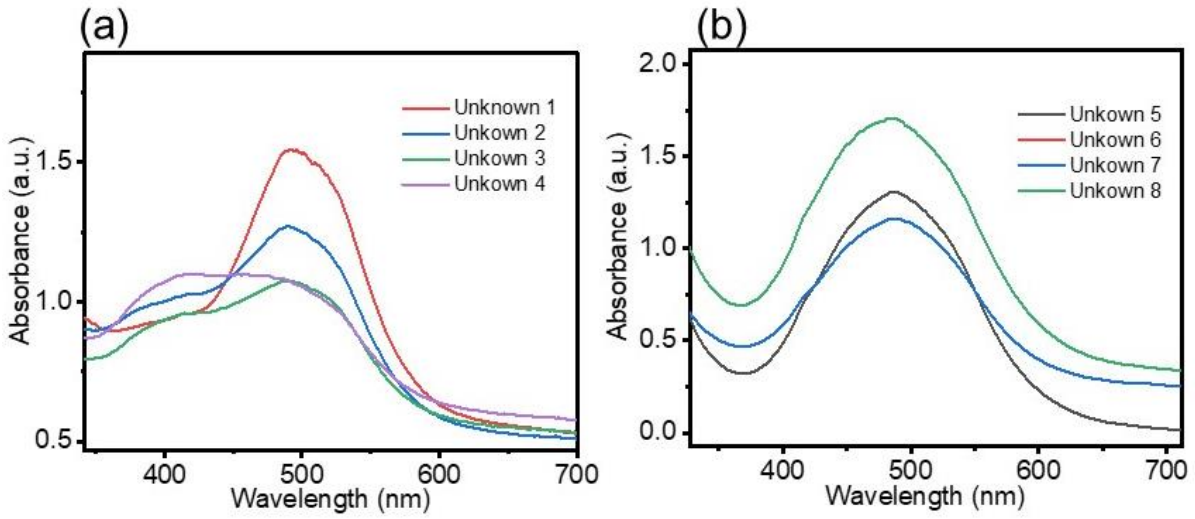

Figure S11. UV-vis spectra recorded for unknown samples by (a) F1 +Au (III) and (b) F2 +Au (III).

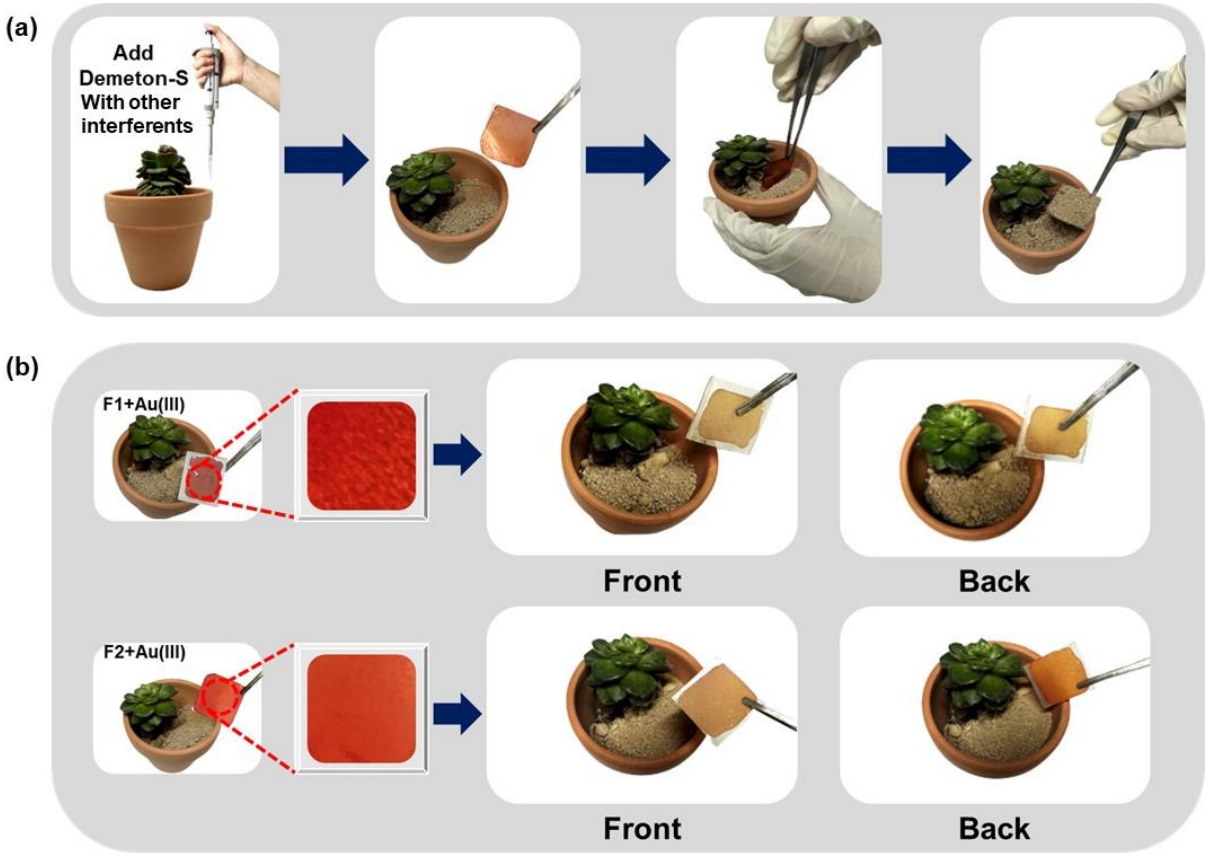

Figure S12. (a) Process of soil detection with Demeton-S. (b) Front and back image of films.

Table S3: Comparison Table.

S.No.	System	Detection Method	Detection Media	Selectivity	Practical Application (Quantification)	Ref
1.	Zirconium MOF	Detection of degraded product	Buffer water	Not shown	Not Shown	[7]
2.	Short wavelength inner filter technique (SWIFT)	Detection of degraded product	Mixed solvent	Both V and G type nerve agent	Not shown	[8]
3.	Chromogenic Small molecule	Detection of hydrolyzed product	Organic Solvent	Both V and G type nerve agent	Not shown	[9]
4.	Chromo-fluorogenic small-molecule	Detection by metal displacement mechanism	Organic Solvent	V type nerve agent	Not shown	[10]
5.	Fluorophore-Lanthanide Complexation	Detection by metal displacement mechanism	Mixed organic solvent	V type nerve agent	Not shown	[11]
6.	Polymeric Film	Detection by Au (III) displacement mechanism	Water Soil Skin	V type nerve agent	Quantification Shown	This Work

References

1. Thiermann, H.; Worek, F.; Kehe, K., Limitations and challenges in treatment of acute chemical warfare agent poisoning. *Chem. Biol. Interact.* **2013,** *206* (3), 435-43.

2. Kim, K.; Tsay, O. G.; Atwood, D. A.; Churchill, D. G., Destruction and Detection of Chemical Warfare Agents. *Chem. Rev.* **2011,** *111* (9), 5345-5403.

3. De Koning, M. C.; Ma, K.; van Grol, M.; Iordanov, I.; Kruijne, M. J. L.; Idrees, K. B.; Xie, H.; Islamoglu, T.; Bross, R. P. T.; Farha, O. K., Development of a Metal Organic Framework/Textile Composite for the Rapid Degradation and Sensitive Detection of the Nerve Agent VX. *Chem. Mater.* **2022,** *34* (3), 1269-1277.

4. Ha, S.; Lee, M.; Seo, H. O.; Song, S. G.; Kim, K. s.; Park, C. H.; Kim, I. H.; Kim, Y. D.; Song, C., Structural Effect of Thioureas on the Detection of Chemical Warfare Agent Simulants. *ACS Sens.* **2017,** *2* (8), 1146-1151.

5. Cai, Y. C.; Li, C.; Song, Q. H., Selective and visual detection of a nerve agent mimic by phosphorylation and protonation of quinolin oximes. *J. Mater. Chem. C* **2017,** *5* (29), 7337-7343.

6. Chen, L.; Wu, D.; Yoon, J., Recent Advances in the Development of Chromophore-Based Chemosensors for Nerve Agents and Phosgene. *ACS Sens.* **2018,** *3* (1), 27-43.

7. Burnworth, M.; Rowan, S. J.; Weder, C., Fluorescent sensors for the detection of chemical warfare agents. *Chemistry* **2007,** *13* (28), 7828-36.

8. Royo, S.; Martínez Máñez, R.; Sancenón, F.; Costero, A. M.; Parra, M.; Gil, S., Chromogenic and fluorogenic reagents for chemical warfare nerve agents' detection. *Chem. Commun.* **2007,** (46), 4839-4847.

9. Sambrook, M. R.; Notman, S., Supramolecular chemistry and chemical warfare agents: from fundamentals of recognition to catalysis and sensing. *Chem. Soc. Rev.* **2013,** *42* (24), 9251-9267.

10. Dennison, G. H.; Sambrook, M. R.; Johnston, M. R., VX and VG chemical warfare agents bidentate complexation with lanthanide ions. *Chem. Commun.* **2014,** *50* (2), 195-197.

11. Kranawetvogl, A.; Küppers, J.; Siegert, M.; Gütschow, M.; Worek, F.; Thiermann, H.; Elsinghorst, P. W.; John, H., Bioanalytical verification of V type nerve agent exposure: simultaneous detection of phosphonylated tyrosines and cysteine-containing disulfide-adducts derived from human albumin. *Anal. Bioanal. Chem.* **2018,** *410* (5), 1463-1474.

12. Kapp, R. W., Book Review: Handbook of Toxicology of Chemical Warfare Agents Third Edition. *Inter. J. Toxi.* **2021,** *40* (3), 299-300.

13. de Koning, M. C.; Peterson, G. W.; van Grol, M.; Iordanov, I.; McEntee, M., Degradation and Detection of the Nerve Agent VX by a Chromophore-Functionalized Zirconium MOF. *Chem. Mater.* **2019,** *31* (18), 7417-7424.

14. Kumar, V.; Raviraju, G.; Rana, H.; Rao, V. K.; Gupta, A. K., Highly selective and sensitive chromogenic detection of nerve agents (sarin, tabun and VX): a multianalyte detection approach. *Chem. Commun.* **2017,** *53* (96), 12954-12957.

15. Joshi, K. A.; Prouza, M.; Kum, M.; Wang, J.; Tang, J.; Haddon, R.; Chen, W.; Mulchandani, A., V Type Nerve Agent Detection Using a Carbon Nanotube Based Amperometric Enzyme Electrode. *Anal. Chem.* **2006,** *78* (1), 331-336.

16. Bazire, A.; Gillon, E.; Lockridge, O.; Vallet, V.; Nachon, F., The kinetic study of the inhibition of human cholinesterases by demeton-S-methyl shows that cholinesterase-based titration methods are not suitable for this organophosphate. *Toxicol. In Vitro.* **2011,** *25* (3), 754-759.

17. Steiner, W. E.; Klopsch, S. J.; English, W. A.; Clowers, B. H.; Hill, H. H., Detection of a Chemical Warfare Agent Simulant in Various Aerosol Matrixes by Ion Mobility Time of Flight Mass Spectrometry. *Anal. Chem.* **2005,** *77* (15), 4792-4799.

18. Khan, M. A.; Long, Y. T.; Schatte, G.; Kraatz, H. B., Surface studies of aminoferrocene derivatives on gold: electrochemical sensors for chemical warfare agents. *Anal. Chem.* **2007,** *79* (7), 2877-84.

19. Steiner, W. E.; Clowers, B. H.; Haigh, P. E.; Hill, H. H., Secondary ionization of chemical warfare agent simulants: atmospheric pressure ion mobility time of flight mass spectrometry. *Anal. Chem.* **2003,** *75* (22), 6068-76.

20. Basha, S. K.; Lakshmi, K. V.; Kumari, V. S., Ammonia sensor and antibacterial activities of green zinc oxide nanoparticles. *Sens. Bio. Sens. Res.* **2016,** *10*, 34-40.

21. Kumar, V.; Kim, H.; Pandey, B.; James, T. D.; Yoon, J.; Anslyn, E. V., Recent advances in fluorescent and colorimetric chemosensors for the detection of chemical warfare agents: a legacy of the 21st century. *Chem. Soc. Rev.* **2023,** *52* (2), 663-704.

22. Bauri, K.; Saha, B.; Mahanti, J.; De, P., A nonconjugated macromolecular luminogen for speedy, selective and sensitive detection of picric acid in water. *Polym. Chem.* **2017,** *8* (46), 7180-7187.

23. Zhu, M.; Sun, L.; Liu, X.; Pang, X.; Fan, F.; Yang, X.; Hua, R.; Wang, Y., A reversible CHEF-based NIR fluorescent probe for sensing Hg2+ and its multiple application in environmental media and biological systems. *Sci. Total Environ.* **2023,** *874*, 162460.

24. Kim, S. K.; Gupta, M.; Lee, H. i., A recyclable polymeric film for the consecutive colorimetric detection of cysteine and mercury ions in the aqueous solution. *Sens. Actuators B Chem.* **2018,** *257*, 728-733.

25. Liu, X.; Shi, T.; Xu, C.; Zhu, M.; Wang, Y., A highly selective and sensitive ICT-based Cu2+ fluorescent probe and its application in bioimaging. *Ecotoxicol. Environ. Saf.* **2023,** *262*, 115127.

26. Jiang, X.; Gao, H.; Zhang, X.; Pang, J.; Li, Y.; Li, K.; Wu, Y.; Li, S.; Zhu, J.;

Wei, Y.; Jiang, L., Highly-sensitive optical organic vapor sensor through polymeric swelling induced variation of fluorescent intensity. *Nat. Commun.* **2018,** *9* (1), 3799.

27. Wang, Y.; Zhu, M.; Shi, T.; Ma, X.; Wu, X.; Li, Q. X.; Hua, R., Construction of a novel fluorescent nanocarrier with double hollow shells for pH-controlled release of imidacloprid and its distribution and transport in bok choy. *Ecotoxicol. Environ. Saf.* **2022,** *246*, 114132.

28. Kumar, V.; Maiti, B.; Chini, M. K.; De, P.; Satapathi, S., Multimodal Fluorescent Polymer Sensor for Highly Sensitive Detection of Nitroaromatics. *Sci. Rep.* **2019,** *9* (1), 7269.

29. Cai, Y. C.; Li, C.; Song, Q. H., Fluorescent Chemosensors with Varying Degrees of Intramolecular Charge Transfer for Detection of a Nerve Agent Mimic in Solutions and in Vapor. *ACS Sens.* **2017,** *2* (6), 834-841.

30. Hu, Z.; Yang, T.; Liu, J.; Zhang, Z.; Feng, G., Preparation and application of a highly sensitive conjugated polymer-copper (II) composite fluorescent sensor for detecting hydrazine in aqueous solution. *Talanta* **2020,** *207*, 120203.

31. Bott Neto, J. L.; Martins, T. S.; Buscaglia, L. A.; Santiago, P. V. B.; Fernández, P. S.; Machado, S. A. S.; Oliveira Jr, O. N., A portable system for photoelectrochemical detection of lactate on TiO2 nanoparticles and [Ni(salen)] polymeric film. *Sens. Actuators B Chem.* **2021,** *345*, 130390.

32. Riccio, B. V. F.; Silvestre, A. L. P.; Meneguin, A. B.; Ribeiro, T. C.; Klosowski, A. B.; Ferrari, P. C.; Chorilli, M., Exploiting Polymeric Films as a Multipurpose Drug Delivery System: a Review. *AAPS Pharm. Sci. Tech.* **2022,** *23* (7), 269.

33. Bak, J. M.; Jung, S. H.; Lee, H.-i., Reusable polymeric films for fluorometric Al3+ detection in anti-counterfeiting and security applications. *Sens. Actuators B Chem.* **2021,** *345*, 130420.

34. Balamurugan, A.; Lee, H. i., Aldoxime-Derived Water-Soluble Polymer for the Multiple Analyte Sensing: Consecutive and Selective Detection of Hg2+, Ag+, ClO–, and Cysteine in Aqueous Media. *Macromolecules* **2015,** *48* (12), 3934-3940.

35. Zhou, W.; Saran, R.; Liu, J., Metal Sensing by DNA. *Chem. Rev.* **2017,** *117* (12), 8272-8325.

36. Gupta, M.; Balamurugan, A.; Lee, H. i., Azoaniline-based rapid and selective dual sensor for copper and fluoride ions with two distinct output modes of detection. *Sens. Actuators B Chem.* **2015,** *211*, 531-536.

37. Balamurugan, A.; Lee, H. i., Single molecular probe for multiple analyte sensing: Efficient and selective detection of mercury and fluoride ions. *Sens. Actuators B Chem.* **2015,** *216*, 80-85.

38. Sharma, R.; Suhendra, N. F.; Jung, S. H.; Lee, H. i., Gold recovery at ultra high purity from electronic waste using selective polymeric film. *J. Chem. Eng.* **2023,** *451*, 138506.

39. Barba-Bon, A.; Costero, A. M.; Gil, S.; Sancenón, F.; Martínez-Máñez, R., Chromo-fluorogenic BODIPY-complexes for selective detection of V-type nerve agent surrogates. *Chem.*

Commun. **2014,** *50* (87), 13289-13291.

Korean abstract

V-시리즈 신경가스(VX)의 신속한 감지와 정량 분석은 지역 갈등 사건, 테러 행위 또는 불법 활동의 예방을 위해 중요합니다. 그러나 VX의 낮은 증발성과 높은 독성으로 인해 이러한 작업들은 어렵습니다. 본 연구에서는 오염된 지역에서 VX 모방물질인 demeton-S를 신속하고 민감하게 감지하기 위해 두 개의 새로운 비색 고분자 필름을 설계했습니다. 이 고분자 필름은 특히 금(Au) 이온을 위한 coordination site를 포함하도록 디자인되었습니다. 초기에는 이러한 필름이 금(Au) 이온과 결합해 분자 내 전하 이동 과정이 향상되어 색상이 변화했습니다. demeton-S가 존재하는 경우 필름 내의 금(Au) 이온 리간드가 demeton-S로 치환되어 분자 내 전하 이동 과정이 억제되어 필름의 원래 색상으로 복원되어 demeton-S의 존재를 표시하는 지표로 작용했습니다. 이 고분자 필름은 G형 신경가스 및 다른 간섭물에 비해 demeton-S에 대한 탁월한 선택성을 나타내었습니다. 더불어, Au (III) 및 demeton-S에 대한 교대 노출 동안 필름의 가역성으로 인해 demeton-S 감지를 위한 고분자필름의 재사용이 가능했습니다. 이 고분자 필름은 다양한 수질, 토양 및 피부 등 여러 오염 지역에서 demeton-S의 감지 및 정량 분석에 적용 가능성을 보여주어 현장에서의 측정에 매우 적합하다는 것을 입증했습니다.